2013

Modeling Of Legged Locomotion With A Suspended Load In The Sagittal Plane

Karna P. Potwar
Purdue University

Graduate School ETD Form 9
(Revised 12/07)

PURDUE UNIVERSITY
GRADUATE SCHOOL
Thesis/Dissertation Acceptance

This is to certify that the thesis/dissertation prepared

By Karna Potwar

Entitled
MODELING OF LEGGED LOCOMOTION WITH A SUSPENDED LOAD IN THE SAGITTAL PLANE

For the degree of Master of Science in Mechanical Engineering

Is approved by the final examining committee:

Justin Seipel
Chair

John M. Starkey

Charles M. Krousgrill

To the best of my knowledge and as understood by the student in the *Research Integrity and Copyright Disclaimer (Graduate School Form 20)*, this thesis/dissertation adheres to the provisions of Purdue University's "Policy on Integrity in Research" and the use of copyrighted material.

Approved by Major Professor(s): Justin Seipel

Approved by: David C. Anderson 12/05/2013
Head of the Graduate Program Date

MODELING OF LEGGED LOCOMOTION WITH A SUSPENDED LOAD IN THE SAGITTAL PLANE

A Thesis

Submitted to the Faculty

of

Purdue University

by

Karna Potwar

In Partial Fulfillment of the

Requirements for the Degree

of

Master of Science in Mechanical Engineering

December 2013

Purdue University

West Lafayette, Indiana

ACKNOWLEDGMENTS

I would like to thank my parents for allowing me to continue my education and pursue my Master's at Purdue University.

I am grateful to carry out my thesis under the supervision of Professor Justin Seipel. His input regarding the field of Bio-Robotics, especially in the area of Human Locmotion, helped me shape my thesis.

Secondly, I would like to acknowledge Jeffrey Ackerman for being a helpful mentor and overseeing my work. His exceptional ability in paraphrasing and explanatory skills have helped me a lot to understand the subject matter.

Thirdly, the countless problem solving sessions with Zhuohua Shen on programing using MATLAB have been essential. They have helped me improve my coding skills and abillity to troubleshoot codes effectively.

I would also like to mention Nikhil Rao who helped me learn LaTeX which helped me organize my thesis.

Lastly to everyone who has been there at Purdue University with me through thick and thin. Thank you, everyone.

TABLE OF CONTENTS

Page

Page

LIST OF TABLES

LIST OF FIGURES

SYMBOLS

m	Body Mass
M	Load Mass
k	Leg Stiffness
l_o	Leg Length
l_{stride}	Stride Length
l	Variable Leg Length
β	Leg Angle w.r.t. Horizontal
c	Leg Damping
τ	Hip Torque
K	Suspension Stiffness
$K_{resonance}$	Suspension Stiffness at Resonance
f	Initial Foot Contact Coordinate
B	Suspension Damping
v_o	Body Mass Velocity
δ	Body Velocity Angle from the Horizontal
F_T	Force due to Hip Torque
F_L	Force due to Leg Compression
F_V	Force due to Load on the Body
x_f	Foot Horizontal Coordinate
y_f	Foot Vertical Coordinate
x	Body Horizontal Displacement
$\dot{x}$	Horizontal Velocity of the Body
y	Body Vertical Displacement
$\dot{y}$	Vertical Velocity of the Body
y_u	Load Displacement

$\dot{y_u}$	Load Velocity
τ_v	Variable Torque
g_τ	Gain Torque
v_t	Target Velocity
ω, ω_{strd}	Stride Frequency
sf	Stride Frequency (Hz)
ω_n	Natural Frequency of Load
ω_d	Damped Natural Frequency of Load
N	Period Cycles
D	Outer Diameter of the Bamboo
d	Inner Diameter of the Bamboo
t	Thickness of the Bamboo
σ_b	Bending Stress
σ_{uts}	Ultimate Tensile Strength
$n_{fracture}$	Factor of Safety Against Fracture
M_b	Bending Moment
I	Moment of Inertia
E	Modulus of Elasticity of the bamboo
G	Shear Modulus of the bamboo
θ_{def}	Angular Deflection of the Pole
K_{eff}	Effective Bamboo Stiffness
Δ	Deflection of the Pole
Δ_{ss}	Deflection of the simply supported beam
K_{ss}	Stiffness of the simply supported beam
I_{ss}	Moment of Inertia of the simply supported beam
E_{ss}	Modulus of Elasticity of the simply supported beam

ABBREVIATIONS

PVC	Poly Vinyl Chloride
DOF	Degree of Freedom
fp,FP	Fixed Points

ABSTRACT

Potwar, Karna M.S.M.E, Purdue University, December 2013. Modeling of Legged Locomotion with a Suspended Load in the Sagittal Plane. Major Professor: Justin E. Seipel, School of Mechanical Engineering.

Walking or running while carrying loads has always been a tedious task, more so when the loads are heavy. Such a task of carrying loads not only requires extra effort but also leads to physical pain and in some cases injury. Prior studies on human locomotion with a suspended load have used models that are restricted in their DOFs and so are not able to take into account the fore aft movement in human beings. The objective of this thesis is to model the dynamics of sagittal plane center-of-mass locomotion with a suspended load and apply findings to carrying loads with an elastic pole.

The approach taken was to develop and analyze a variant of the Hip Actuated Spring-Loaded Inverted Pendulum (SLIP) model of locomotion that has a second sprung mass added to represent a suspended load. This model showed a large increment in human running speed and stride frequency as the suspension stiffness was increased. A stability analysis on the model showed branching among fixed points with one branch nearly stable while the other branch has greater stability. This particular model was able to show a reduction in peak forces and amplitude of the load for very compliant suspensions.

In order to limit velocity change that occurs with changing suspension stiffness, a variable torque model was developed. This model was able to limit the velocity magnitude and stride frequency near target values. It also showed reduction in peak shoulder forces and has better stability.

One direct application of this work is to inform and potentially influence better practices involving the ancient human behavior of carrying heavy loads with bamboo

poles, which remains common in some regions of Asia. The dynamic aspects of the hip actuated SLIP were synthesized with those of the beam bending model to design a compliant pole. Optimizing the design parameters of bamboo helped us to obtain a region which provided suitable reduction in peak shoulder forces within the safety limits of avoiding fracture.

1. INTRODUCTION

Humans tend to modify their gait while carrying loads. The extent of the modification depends on mass of the load and the away it is being carried [1]. Elasticity being a fundamental property of legged locomotion, human leg elasticity is actively regulated [2]. Elastically suspended loads are known to be able to reduce the metabolic cost of energy along with reduction of peak forces experienced by the body, relative to carrying a load rigidly attached to the body [3, 4]. Rome et.al. has also shown reduction in peak shoulder forces by around 33% and in the energetic cost of locomotion by 6.2 % by carrying load suspended through rubber bands. Kram et al. showed using a complaint pole system to carry heavy loads decreased shoulder forces as seen in Figure 2.10. Knapik et.al. suggested usage of front-back backpacks as the load gets distributed evenly along the shoulders and the person carrying doesn't need to lean forward [5]. He also suggested that there should be hip harness for backpacks which helps in redistributing the load on the shoulders onto the lower extremity thereby easing the stress on the human back.

Many single and double DOF models have been developed to further study the dynamics of elastically suspended load on legged locomotion. As most of them do not take into consideration the fore aft movement of human locomotion the results are restricted to the vertical dynamics of locomotion. Regardless, a double mass hopper for legged locomotion in robots was able to predict reduction in peak forces along with power consumption [6]. However, a more sophisticated model including the fore aft dynamics is required which can more accurately be compared with human legged locomotion. To model the sagittal plane dynamics of locomotion, including both vertical and fore-aft motion, the Spring Loaded Inverted Pendulum is one of the most robust model which has been developed to study this phenomenon [7, 8]. In order to study the dynamics of suspended loads on the human body, an extra mass

was added to this SLIP model which adds an extra degree of freedom. This nonlinear variant had a passive suspension attached to the actuated mass. Using this model we investigated the effects of varying the stiffness and damping of the suspension on human motion.

1.1 Problem Statement

The purpose of this thesis is to analyze the effects of a suspended load on the vertical and fore aft movement in human locomotion. The objectives of this study are as follows:

1. To understand the effects of coupled dynamics between the load and body on the forward velocity and stride frequency.

2. To analyze the stability of this sagittal plane locomotion model.

1.2 Hypothesis

1. A heavy load attached rigidly or elastically to the human body can affect the speed and gait of locomotion in human beings. Specifically, the forward velocity and stride frequency.

2. Avery low stiffness suspension with insufficient damping can cause instability to the human legged locomotion.

2. BACKGROUND AND LITERATURE SURVEY

2.1 Human Body Planes

The human body can be projected onto three separate planes, namely the sagittal, transverse and coronal planes. Each plane is useful in it's own way to characterize and analyze human body movements. The transverse plane will be useful in observing yawing dynamics of the upper body; the coronal plane for upper body's side tilting or rolling, along with lateral movements of arms and legs. The sagittal plane helps in detecting fore aft movement of the body and pitching dynamics of the body. Figure 2.1 shows the division of the human body by the three planes described here.

2.1.1 Human Body Segmentation and Movement

In order to facilitate the study of dynamics of the human skeleton it is necessary to figure out the internal forces and the actuations that lead to body movements. The human body is divided into upper and lower body. The lower body is responsible for providing actuation to move over ground such as walking, jogging, running and sprinting, while the upper body acts as a stabilizing agent. The upper torso undergoes pitching, rolling and yawing which may either actively or passively affects human locomotion. The arm swings counteract the yawing that is generated due to locomotion by providing a reverse torque so as to prevent the yawing about the craniocaudal axis. This anti-torque cancels the yawing of the body that is generated due to human locomotion. During walking or running the hip torque creates a couple about the Left-right Axis causing pitching in the body. This pitching, also like the arm swings, adds stability to locomotion.

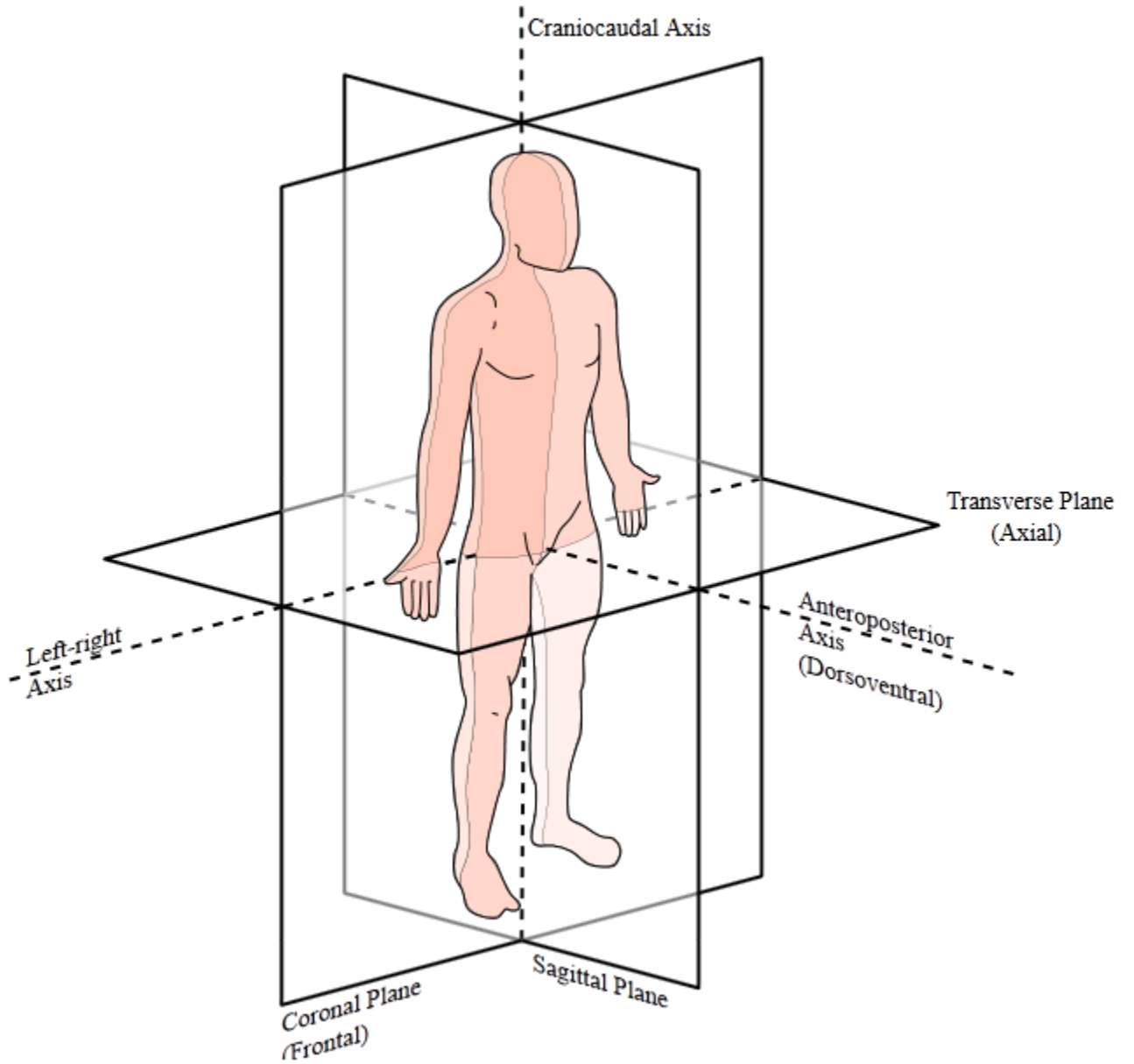

Figure 2.1. 3-Dimensional Representation of the Human Body. Reproduced from [9].

2.1.2 Actuation and Joint Torques

The human skeleton is held together through inter-connected networks of muscles and ligaments. Muscles and ligaments are elastic in nature and so are capable of

storing elastic energy when stretched. They, in turn, help in joint movements and actuation, which is necessary for locomotion [10]. The bones act as links and are connected to adjacent bones through joints. The human body possesses various joints required to carry out movement. Such as the hinge joint seen in the elbow and knee, and the ball and socket joint in the shoulder and hip joint. The wrist and the ankle joints are a collection of interwoven muscle fibers called ligaments, tendons and cartilages which provide the necessary 3D movement. The primary movement in the ankle joint can be projected onto the sagittal plane which is responsible for providing requisite torque for locomotion. The viscoelastic nature of the muscles which also helps in providing stability to the body by loosening or tightening. These two muscular actions aid in maintaining a stable posture and also affect locomotion. Thus, muscles are an integral part of human body movements.

Actuation and magnitude of torque generated in the various joints depends on the length and density of the muscle fiber. The hip generates about 40-80 Nm of torque, with the knee generating 125-273 Nm and the ankle around 180-240 Nm [11].The contribution of these torques isn't constant throughout there active state. They vary based on the speed of locomotion, the power required and the weight being carried. As seen in Figure 2.2 we can see the way the torque varies during the time the foot/prosthetic limb is in contact with the ground. From this figure we see that the hip moment is maximum at the beginning of the stride while the ankle moment is maximum at 50 % completion of the stride. This shows the torque vary with percent stride completion in order to maintain a constant speed.

2.2 Lower Body Mechanics and Properties

The human lower body consists mainly of the hip, leg and the ankle. The muscles in the legs and the hip are capable of storing energy due to their viscoelastic properties. During walking and running the energy accumulated by the calf muscles in the first half of the stride is released during the second half of the stride. So along with joint

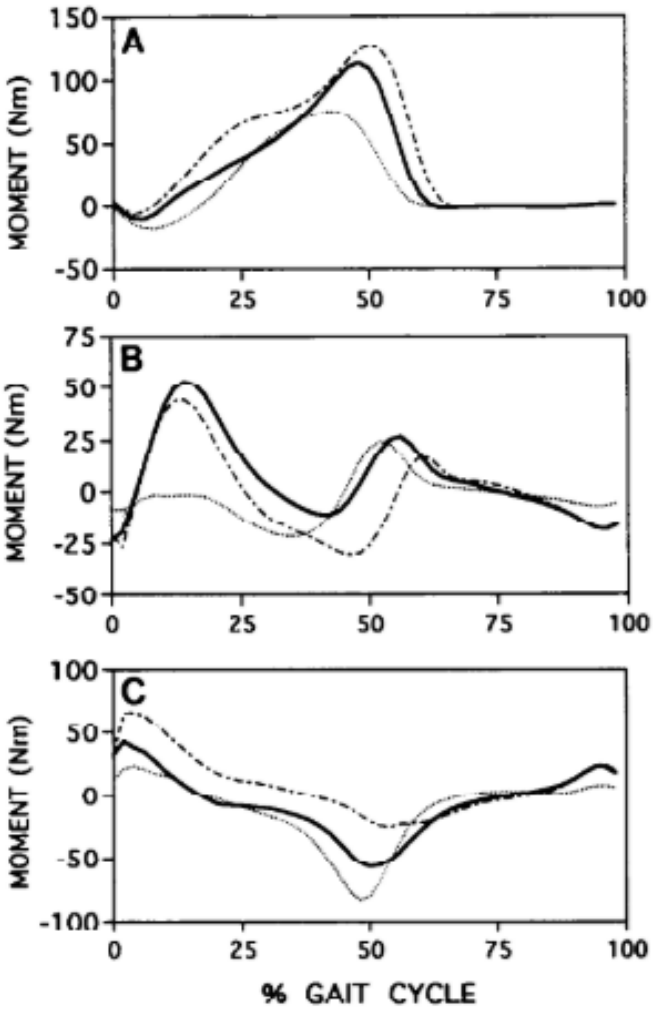

Figure 2.2. Torque Profiles of Ankle, Knee and Hip for a Normal Person(solid line) versus an intact limb(dot-dash) and a Prosthetic Limb (dotted). Reproduced from [12].

torques the stored energy acts towards human locomotion. This energy provides an upward thrust aiding running. The lower body dynamics can mainly be monitored in the sagittal plane as it best describes the fore aft movement characteristic of forward movement. Figure 2.3 shows the meshing of the muscles along the leg which provide structural stability to the human leg. The anchor representing the human leg with the joint torques can be seen in Figure 2.4. All three moments about the three leg

joints provide the torque in the same direction. An equivalent model with just the hip torque can be developed by lumping the individual joint torques into the hip torque as seen in Figure 2.4.

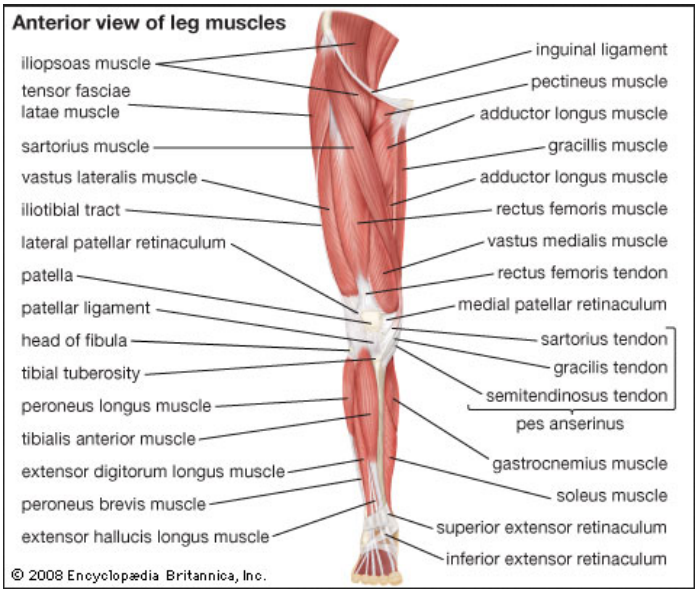

Figure 2.3. Muscle Network in the Human Leg. Reproduced from [13].

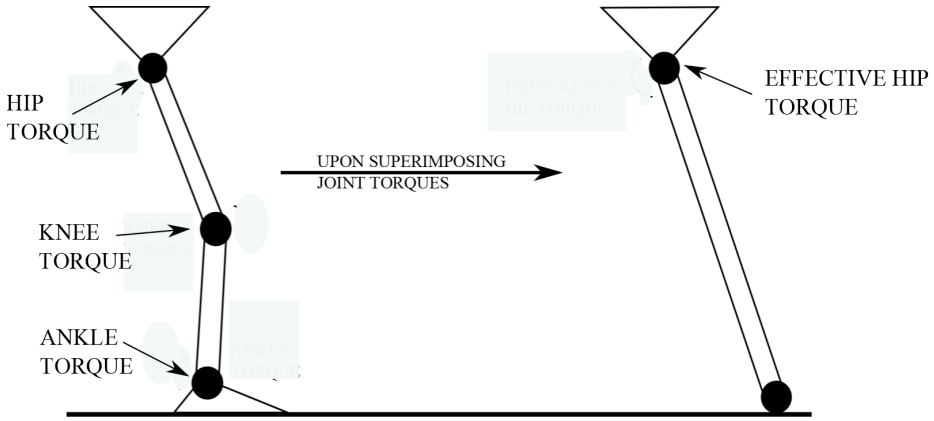

Figure 2.4. Joint Torques in the Leg as Seen in the Sagittal Plane, Lumped to an Effective Hip Actuated Anchor.

2.2.1 Viscoelasticity of the Human Leg

Locomotion apart from joint moments requires storage of energy. This can be seen from the fact that a human goes air borne as he or she starts to run. Unlike walking, running portrays flight phases which can be achieved if there is an upward thrust provided towards the end of the stance phase. This lift off is achieved due in part to the elastic nature of muscular fibers. They store energy when the leg touches the ground by undergoing compression and release the energy when the leg is about to lift off. This release of energy is greater during running compared to walking. In walking as soon as or just before one of the legs is about to lift off, the second leg touches down.

Farley et al. showed that the human leg stiffness increases as the stride frequency increases [14, 15]. Figure 2.6 shows the variation in human leg stiffness upon change in stride frequency. The human leg shows variable stiffness for hopping as well, as shown by Rapoport et al. For hopping the stiffness of ankle depends on the angular deflection of the ankle w.r.t. the leg and also of the hip w.r.t. the knee [16]. A runner can perform better on a more compliant surface compared to hard surfaces. This compliant surface will store energy from the runner and transmit it back to the runner, which reduces the effort put in by the runner [17]. Thus lower muscular force requirement and work generation will help the runner lose less energy as compared to running on hard surfaces.

The viscoelastic nature of the leg provides the necessary energy storage which is required during running. But if the extra energy that gets stored in the muscles is not properly dissipated the body might traverse larger amplitudes while running. Apart from storing energy the body also dissipates extra energy that gets transmitted due to muscle actuation. Zhang et al. showed that the human leg has inherent damping apart from a leg stiffness. He used three subjects who stood on an AMTI force platform and their center of mass was moved up and down. Without damping, the body would have bounced endlessly [18]. He showed using a single mass spring damper model

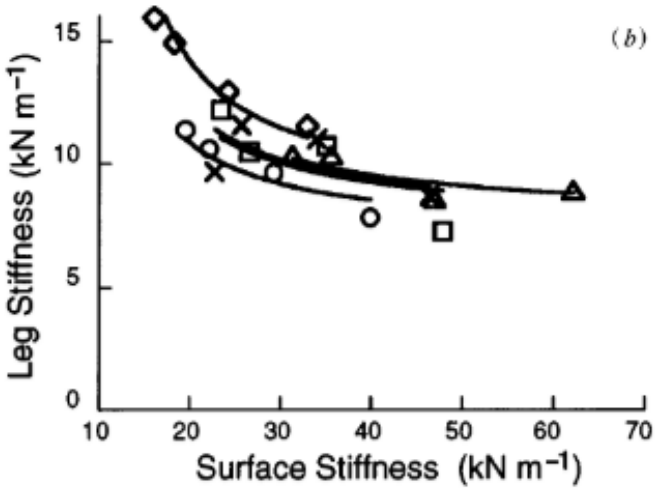

Figure 2.5. Variation in Human Leg Stiffness Depending on the Surface Stiffness. Reproduced from [17].

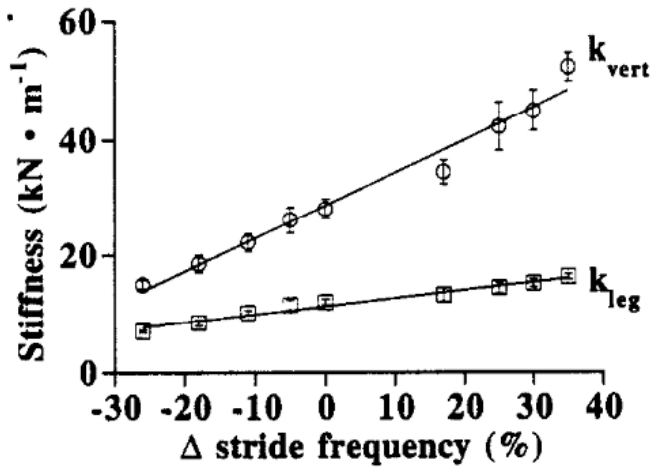

Figure 2.6. Change in Vertical and Human Leg Stiffness upon Variation in Stride Frequency. Reproduced from [14].

that the human leg stiffness is 28000 N/m and the damping is 950 Ns/m. Shen et al. showed that the damping in an actuated SLIP(Spring Loaded Inverted Pendulum) model is directly proportional to the hip torque [7].

2.3 Templates for Studying Human Locomotion

In order to study and analyze human body locomotion, many templates have been developed. Templates are simple spring mass models which help in qualitative assessment of the system under study. There simplicity helps in using them to model various organisms [19].

2.3.1 Hopper Model

This template is the simplest among all the templates used to analyze human motion. It has a mass attached to a spring and a damper. It is given a suitable force excitation depending on the physical activity being studied. The force excitation can be a step impulse or a sinusoidal wave. This model has a single DOF which can help model human hopping. Xhang et al. used such a model to evaluate human leg stiffness as discussed in the previous section. Diagram on the left of Figure 2.7 shows a simple hopper model with no base excitation. The sprung mass is considered as the human mass, while the legs are modeled as a spring damper combination in parallel.

To model a human carrying loads requires more sophistication than a single mass hopper model, if the load isn't rigidly attached to the body. For suspended loads an additional load is attached to the actuated body. Ackerman et al. used a double mass hopper model to predict the energetics of a human walking with elastically suspended load as seen in Figure 2.8 [6]. A double mass hopper model was also used by Hoover et al. to characterize force dynamics of a suspended backpack carried while walking [20]. Rahman et al. used a similar system to analyze vibrations generated due to a suspended backpack [21].

2.3.2 Spring Loaded Inverted Pendulum(SLIP)

A wide variety of templates have been developed which take into account the fore aft movement as seen in humans. The hopper model was restricted to only vertical

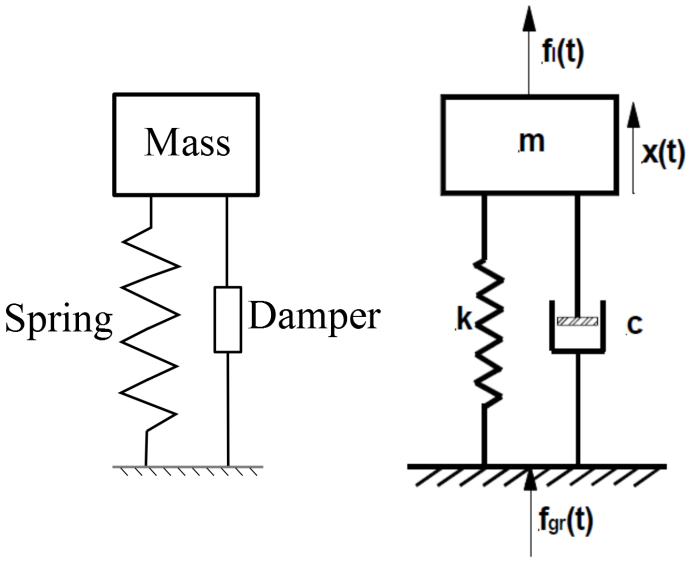

Figure 2.7. (Left) A Spring-Mass-Damper Hopper Model and (Right) a Base Excited Hopper Model. Model on the right is reproduced from [18].

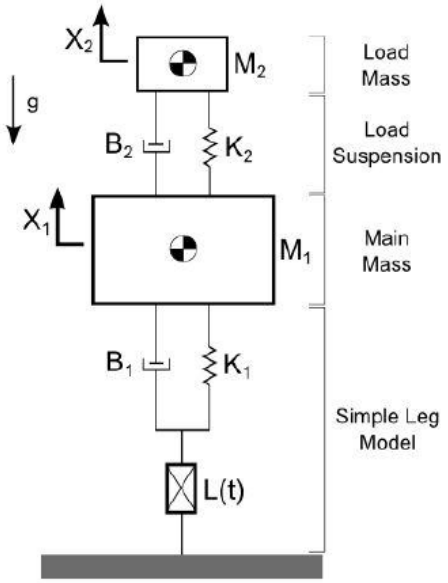

Figure 2.8. A Double Mass Hopper Model used to Simulate Legged Locomotion with Elastically Suspended Loads. Reproduced from [6].

movement and motion against or along the direction of gravitational force. The SLIP model has an extra degree of freedom in the horizontal direction. In the past, energy conservative SLIP(C-SLIP) templates were used to demonstrate walking and running [8, 22, 23]. A C-SLIP works on the principle of conservation of energy. With given initial condition it can propagate endlessly. These C-SLIPs are not stable as compared to actuated SLIP and a small perturbation can easily destabilize them. Due to no energy dissipation or actuation the stability of such a conservative model is restricted. An upgrade of the C-SLIP called the Hip Actuated SLIP was developed by Shen et al. This provided a larger stable regime compared to the conservative model [7]. Please see Figure 2.9.

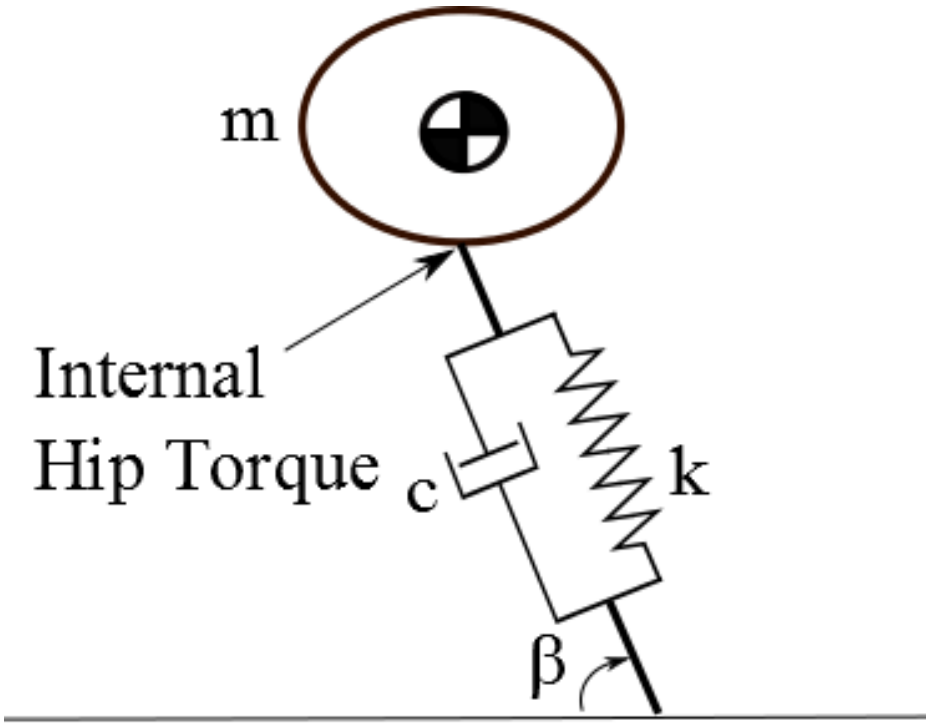

Figure 2.9. A Conservative SLIP model(Left) and a Hip Actuated SLIP model(Right). Reproduced from [24].

2.4 Elastically Suspended Loads

Soldiers tend to carry a heavy backpack which has an approximate mass of 15-20 kg. Such a magnitude of load can cause physical changes to the body like stooping, leaning and modulation of gait [1]. Most of these backpacks are rigidly attached to the person carrying it and move in conjunction with the person. Kram showed that carrying load through compliant poles can help in reduction of peak forces on the shoulders [4]. He showed the benefits of carrying an elastically suspended load versus a rigid load. Foissac et al. characterized the compliant and rigid suspension parameters for backpacks for different running speeds. Hoover et al. also showed reduction in peak forces due to a suspended backpack by modeling the backpack as a single mass model with base excitation. Loading during the stance phase of walking can increase the extensor electromyographic bursts [25]. These extensor muscles are located just above the ankle in the calf muscle complex. Thus loading can increase peak force on the shoulder, increase metabolic cost [3] and can cause fatigue & stress in the leg muscles.

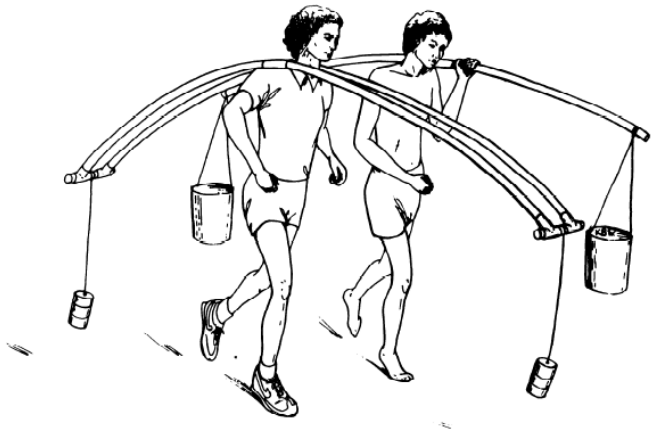

Figure 2.10. Carrying Loads with a Complaint Pole System. Reproduced from [4].

3. APPROACH TAKEN FOR THE STUDY

Human locomotion can be analyzed in three different planes depending on the type of body part under observation. The sagittal plane helps provide a good representation of the human vertical and fore aft movement.

3.1 Modeling the System

As described in Chapter 2, the human system will be modeled as a SLIP model with hip actuation. The upper body in this study is considered as a particle mass. The body mass will have two degrees of freedom in the vertical and the fore aft direction. The leg is reduced to a single link with no ankle or knee. It has a spring to provide elasticity to the system along with a damper. The hip torque provides the necessary initial force to put the body in motion.

The suspension attached to the body mass is modeled using a lumped spring and damper. It is a parallel spring and damper combination with one end attached to the actuated mass and the other end attached to the load being carried.

3.2 Double Mass Hip-SLIP Model

The study uses a HIP-SLIP model as described in chapter 2 with an extra mass atop the actuated mass. It acts as a combination of a double mass hopper model and a single mass HIP-SLIP model. This model is an upgrade of the double mass hopper model as it involves an extra degree of freedom in the fore-aft direction compared to the two degrees of freedom for the hopper model [6, 7]. The load attached to the actuated mass is constrained to move vertically and has no relative motion in the horizontal direction w.r.t. the body mass. At the start of the motion the model is

provided a set of initial conditions which set the system into motion. Please refer Figure 3.1.

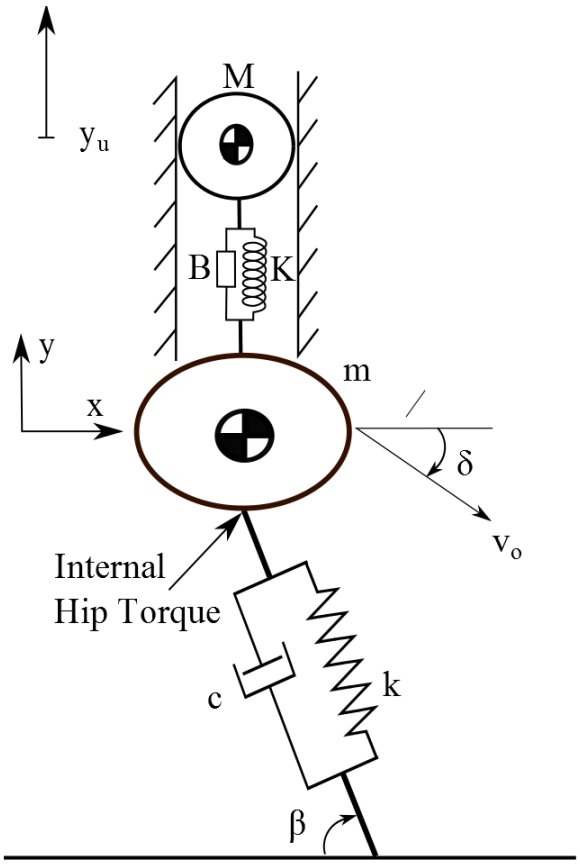

Figure 3.1. Double Mass Hip Actuated-SLIP Model.

3.2.1 Equations of Motion

We employ the Newton-Euler method to derive the equations of motion for this system with the Cartesian Coordinates as the reference frame. The model is a hybrid system which portrays both stance and aerial phases. During stance phase the foot of the Hip-SLIP is in contact with ground and the whole system pivots about this point. The model is a single leg system. Human running doesn't encounter a double stance phase, a single legged Hip-SLIP effectively describes the motion. The free

body diagram of this model can be seen in Chapter 4 Figure 4.1. The stance phase leg length is defined by the equation,

$$l = \sqrt{(x-f)^2 + y^2}, \tag{3.1}$$

where x,y are horizontal and vertical co ordinates while, l and f are leg length and initial stance length respectively. The leg angle θ is defined by

$$\theta = \arctan(\frac{y}{x-f}). \tag{3.2}$$

The constant torque produced at the hipτ, produces a force at the foot contact defined as

$$F_T = \frac{\tau}{l}. \tag{3.3}$$

The leg during stance phase undergoes compression and the force fluctuates as signified by the equation

$$F_L = k(l_o - l) - \frac{c}{l}((x-f)\dot{x} + y\dot{y}), \tag{3.4}$$

where k and c are the leg stiffness and leg damping respectively. Where, $\dot{x}$ and $\dot{y}$ are the forward and vertical velocities respectively. The elastically suspended load experiences a force through the suspension given by

$$F_V = K(y_u - y) + B(\dot{y_u} - \dot{y}), \tag{3.5}$$

with K as the suspension stiffness and B as the suspension damping. With $\dot{y_u}$ as the load velocity and y_u as the load's vertical displacement. The power P required during the stance phase is given by the product of instantaneous angular velocity, $\dot{theta}$ and hip torque

$$P = \tau\dot{\theta}. \tag{3.6}$$

The instantaneous angular velocity $\dot{\theta}$ is given by product of angular velocity and torque

$$\dot{\theta} = (\dot{x}\sin\theta + \dot{y}\cos\theta). \tag{3.7}$$

During the stance phase the acceleration of the body in the fore aft direction is given by

$$\ddot{x} = \frac{(F_T\sin\theta - F_L\cos\theta)}{m}, \tag{3.8}$$

while for it's vertical motion the acceleration is defined as

$$\ddot{y} = \frac{(F_L\sin\theta + F_T\cos\theta + F_V)}{m} - g. \tag{3.9}$$

The load is restricted to move in the vertical direction and accelerates as shown by the equation

$$\ddot{y_u} = \frac{-F_V}{m} - g. \tag{3.10}$$

During stance, the torque τ rotates the leg while the leg is compressed. When the vertical forces at the foot become zero, the system lifts off and enters the flight phase. The ground reaction force at the foot is give by

$$F_L\sin\theta + F_T\cos\theta = 0. \tag{3.11}$$

The model transitions from the flight phase to the stance phase when the leg touches the ground at a given touchdown angle β with the new foot coordinates as $x_f = l_{stride} + l_o\cos\beta$ and $y_f = 0$, with l_{stride} being the stride length of the model.

3.3 Velocity Controlled Actuated SLIP model

The velocity controlled model works on the principle of torque variation throughout the stance phase. This regulation of the torque at the hip helps in achieving a constant forward velocity of the body mass. For this particular model we use a gain torque equation given by

$$\tau_v = g_\tau(v_t - \dot{x}). \tag{3.12}$$

Here, a feedback loop ensures that the forward velocity of the body converges to the desired target velocity, v_t. The variable torque helps in increasing the velocity in the x direction and as the error minimizes the torque value decreases. Unlike the constant torque model which acts as an open loop system, the velocity control model aids in keeping the velocity constant for a larger parameter set.

3.4 Analyzing the Energetics and Stability of the Models

The constant hip torque model will be used to analyze human locomotion with suspended loading and then compared with experimental data along with previous models used to study suspended load locomotion in human beings. Trends in average velocity, stride frequency, body and load trajectories and energetics will be compared with those of the rigidly attached load. Stability analysis of the constant torque model will be carried out through calculation of fixed points so as to interpret the model behavior for highly compliant suspensions.

Similar analysis will be performed on the velocity controlled model. Based on this analysis a suitable model will then be used explain experimental results published by Kram on "Carrying loads with Compliant Poles [4]." Optimizing the parameters of two bamboo species Kao Zhu and Mao Zhu [26] will be done to provide a suitable region in which the peak forces acting on the body from the load are low. This recommended region will be generated through adding constraints, in order to narrow down the diameter and length ranges of the bamboo for which the person carrying the poles would experience minimum shoulder forces.

4. ENERGETICS OF HUMAN RUNNING

This chapter shows the effects of an added mass on the peak shoulder forces experienced by the runner along with the power required for running. The study tries to show the effect of decreasing compliance of the suspension on the dynamics of locomotion .

Elasticity is a fundamental characteristic of legged locomotion and is generally thought to affect the efficiency of motion [2]. Load carried by humans is attached to the body either elastically or rigidly while they run or walk. Rome et al. experimentally demonstrated that human walking with an elastically suspended load backpack reduced the peak forces acting on the human body by 33% and the energetic cost of locomotion by 6.2% compared to walking with a rigidly-attached load [27]. Running with a suspended load backpack reduced the peak forces acting on the human body by 60% compared to running with a rigidly-attached load, but the difference in the energetic cost of running was not reported. Prior to the work by Rome et al., Kram experimentally investigated human running while carrying loads with compliant poles [4]. Kram showed that the peak forces acting on the human body while carrying a load with springy poles were reduced by approximately 40% compared to a standard backpack but reported no significant differences in the energetic cost of running. It is unclear why the energetic cost was reduced for a human walking with a suspended load but not for running. Simple linear single degree of freedom spring-mass models have been developed to investigate locomotion with elastically-suspended loads [20, 28, 29]. These models enable the investigation of the dynamics of the load mass and the peak forces acting on the body. However, they are highly simplified and do not capture the coupled dynamics of the load and the body which could affect locomotion. A linear two degree of freedom spring-mass model was developed [30] which allows the investigation of the coupled dynamics of the load and the body and

enabled an approximation of the energetic cost of walking with a suspended load. This linear model showed that the peak forces of the load on the body and energetic cost of walking are reduced as the suspension stiffness is minimized. The model results were experimentally validated with a legged robot [6]. However, the predictive ability of this linear model may be limited by its simplicity. A nonlinear variant of the two degree of freedom spring-mass model was developed which added a stance and a flight phase, transforming the system into a hybrid nonlinear hopping model [7]. This hybrid nonlinear model was different energetically as compared to the previous linear model due to the addition of a flight phase. While this simple spring-mass hopping model may be qualitatively similar to human hopping, a more advanced model is needed to model human running with an elastically-suspended load.

Therefore, we added a load mass with a suspension attached to the main body of the Actuated SLIP model [7]. We investigated how varying the load suspension stiffness affects the coupled dynamics of the load mass and the body mass, the peak forces of the load on the body, and the average energetic cost of human running.

4.1 Initial Condition and Parameters

In this study, we employ the constant torque equations derived in Chapter 3. An initial velocity $v_o = 3$ m/s was imparted to the system in the touch down phase which was directed downwards from the horizontal at an angle $\delta_o = 10.6^o$ [7]. The touchdown angle was set to $\beta = 65^o$ and the leg length was chosen to be $l_o = 1$ m, which could approximate the leg angle of a running human. It is important to note that the static force M*g of the load deflects the suspension spring. Therefore, the position of the load is centered about its static equilibrium position. Thus, the initial coordinates of the body mass are given by $x_o = 0$, $y_o = l_o \sin(\beta)$ while that of the load is $y_{uo} = y_o - Mg/K$.

The approximate human parameters used are listed in Table 4.1. The stiffness of the human leg is variable and depends on a variety of factors. During running the

Table 4.1.
Approximate Human Parameters.

Parameter	Value
Leg Stiffness, k	13705 N/m
Leg Damping, c	945 Ns/m
Leg Angle, β	65^o
Hip Torque, τ	300 Nm
Body Mass, m	70 kg
Load Mass, M	15 kg

leg stiffness, k, tends to increase while for walking stiffness tends to decrease [14]. An approximate value of 13705 N/m [14] was assumed for the leg with a damping of 950 Ns/m [18]. The mass of the load, M, was set at 15 kg which represents a heavy load that is 21% of the body mass. Due to lack of data on the joint torque required for human running with an elastically-suspended load, we used an estimated value based on data from human running without a load. The human leg during running is powered by torques generated through the hip, knee, and ankle with approximate torque values of 40-80 N-m, 125-273 N-m and 180-240 N-m respectively [11]. We lumped these torque values for the double mass Actuated SLIP model and assumed a constant torque τ= 300 N-m acting on the leg during the stance phase to simulate human running with a 15 kg load. This torque provided stable periodic motion across other parameter variations that we studied. The free body diagram of the body and mass during flight and stance is show in Figure 4.1

To compare human running with an elastically-suspended load versus a rigidly-attached load, we must first establish a definition for a rigidly-attached load. If a load was attached to the body with a perfectly rigid interface, we would assume that the load mass M and the body mass m are lumped into a single effective mass M + m.

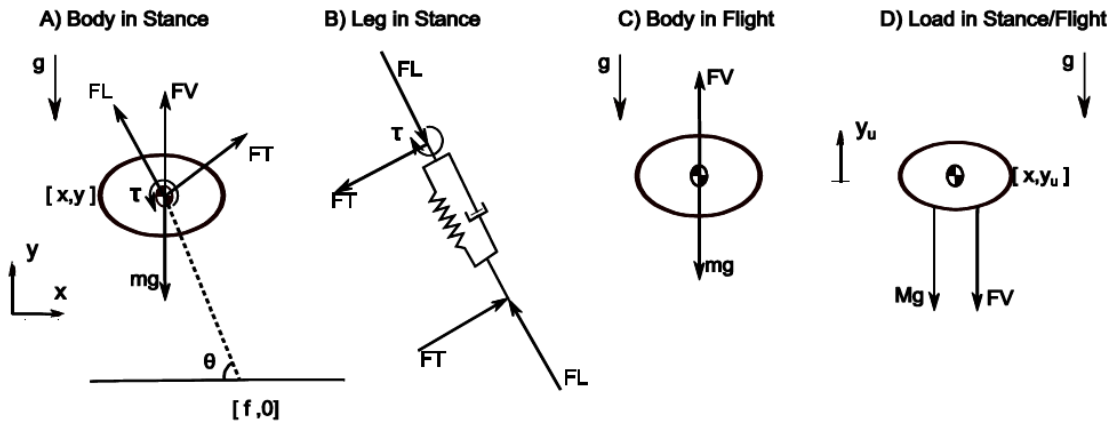

Figure 4.1. Free Body Diagram of the Separate Links Present in the Double Mass Hip-SLIP. Reproduced from [24].

However, this assumption reduces the degrees of freedom of the double mass Actuated SLIP model by one. Thus, we would be comparing a three degree of freedom double mass model to a two degree of freedom single mass model. Assuming a single lumped mass would preclude analysis of the relative forces of the load mass on the body mass. Therefore, we sought to identify suspension stiffness and damping parameters that could approximate a rigidly-attached load.

Foissac et al. characterized the mechanical properties of a typical locked (rigid) backpack and the suspended backpack [29]. The effective suspension stiffness and damping of the rigid and suspended backpack were determined by perturbing the load, measuring the response, and fitting the data to a simple spring-mass-damper model. Foissac reported that the suspension stiffness, K, of the rigid backpack was approximately 51877 N/m and the suspension damping B was 50 N-s/m. However, when the rigid backpack was attached to the human body, the effective stiffness of the rigid backpack was reduced to approximately 5060 N/m and the damping was increased to 320 N-s/m. Moreover, the effective stiffness of the backpack when attached to the human body while walking increased as walking speed increased. The work by Foissac et al. shows that the parameter values for a rigidly-attached load

could vary with different load interface configurations. Further, the effective stiffness and damping of a rigid load can vary when attached to the body while walking at different speeds. No parameter data on running with a rigid load has been reported. Given that there is a high degree of uncertainty in how a rigid load is defined, we decided to define a rigidly-attached load by comparing it to a lumped mass model to generate a conservative estimate. The lumped mass model was simulated with a mass of m + M = 85 kg and the double mass model with a rigid suspension had a load mass M = 15 kg attached to the actuated body mass m = 70 kg.

4.2 Results

4.2.1 Defining a Rigidly Attached Load

A perfectly rigid suspension could be considered to have near-infinite stiffness and damping. After iterating through many different suspension stiffness and damping values, as a conservative estimate of a rigidly-attached load we chose a stiffness K = 500,000 N/m and a damping ratio of 1, or B = 5450 Ns/m for a load mass M = 15 kg. We found that these values closely approximated a rigidly-attached load by comparing the trajectory and speed with a single lumped mass model Figure 4.2.

4.2.2 Stride Frequency and Average Speed of the System

In this model, the average horizontal velocity initial condition for a rigidly-attached load was approximately 3 m/s. The average stride frequency can be estimated from the average horizontal speed

$$sf = \frac{\dot{x}}{l}, \tag{4.1}$$

and the angular stride frequency is given by

$$\omega = 2\pi f. \tag{4.2}$$

The stepping frequency at an average horizontal velocity of 3 m/s was 3.1 Hz or ω = 19.5 rad/s. For a linear model with a single forcing frequency, we would expect

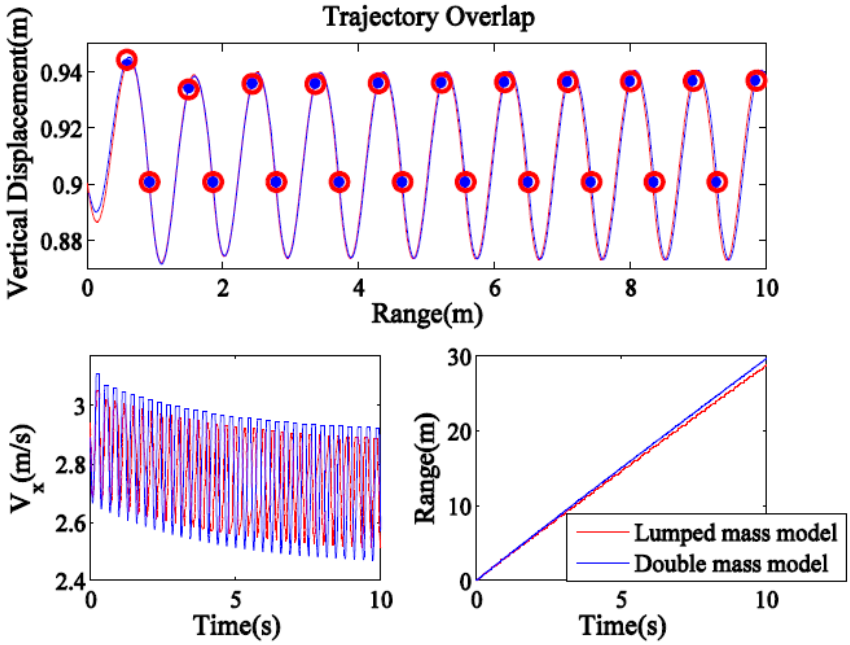

Figure 4.2. Trajectory Overlap of the Rigid Condition with the Lumped Mass Model.

that resonance would occur when the value of f equals ω_n. At resonance, the stepping frequency of the model should excite the resonance condition of the load suspension

$$\omega = \omega_n. \tag{4.3}$$

The load natural frequency can be defined as

$$\omega_n = \sqrt{\frac{K}{M}}. \tag{4.4}$$

From this the suspension stiffness that results in resonance is given by

$$K_{resonance} = m\omega^2. \tag{4.5}$$

For the above frequency, the suspension stiffness, K, that causes resonance for a linear system [30] is approximately 5330 N/m. We expected that this resonant suspension stiffness would serve as a critical point for the system. In the experimental

study of human walking with a suspended backpack by Foissac et al., a suspended backpack had a suspension damping B of approximately 100 N-s/m [29]. Therefore, we tuned the suspension stiffness K = 5330 N/m and chose damping values near B = 100 N-s/m to investigate the dynamics of the system near the resonance condition. The initial model results showed that the predicted resonant suspension stiffness K = 5330 N/m did not exhibit a large amplitude of oscillation for the load mass as would be expected at resonance. Therefore, we conducted a parameter sweep of the suspension stiffness K from 0 to 15000 N/m with a fixed suspension damping B = 100 N-s/m to determine where the actual resonant condition of the system occurs. After the model reached steady state, the average horizontal running speed from one stance phase to the next stance phase was calculated for each suspension stiffness K. The model showed an increase in the average running speed as the suspension stiffness K increased up to some maximum value before converging to the average speed of running with a rigidly-attached load Figure 4.3. The average running speed increased from 3.25 m/s for low suspension stiffness K values and the rigid coupling configuration to approximately 4.5 m/s at a suspension stiffness K = 12000 N/m.

The stride frequency also kept increasing until the load suspension stiffness K = 12600 N/m and abruptly decreased at higher stiffness values, approaching the rigid coupling condition Figure 4.4. The two curves of the stride frequency ω and the natural frequency of the load suspension ω_n almost intersect at the suspension stiffness K where the stride frequency exhibits a peak. This result indicates that the stride frequency of the model is coupled with the natural frequency of the load suspension. The peak in the stride frequency is the actual resonant condition for this coupled system and occurs at a higher suspension stiffness K=12600 N/m than the expected value of K = 5330 N/m at which resonance would have occurred for constant stride frequency in a linear model.

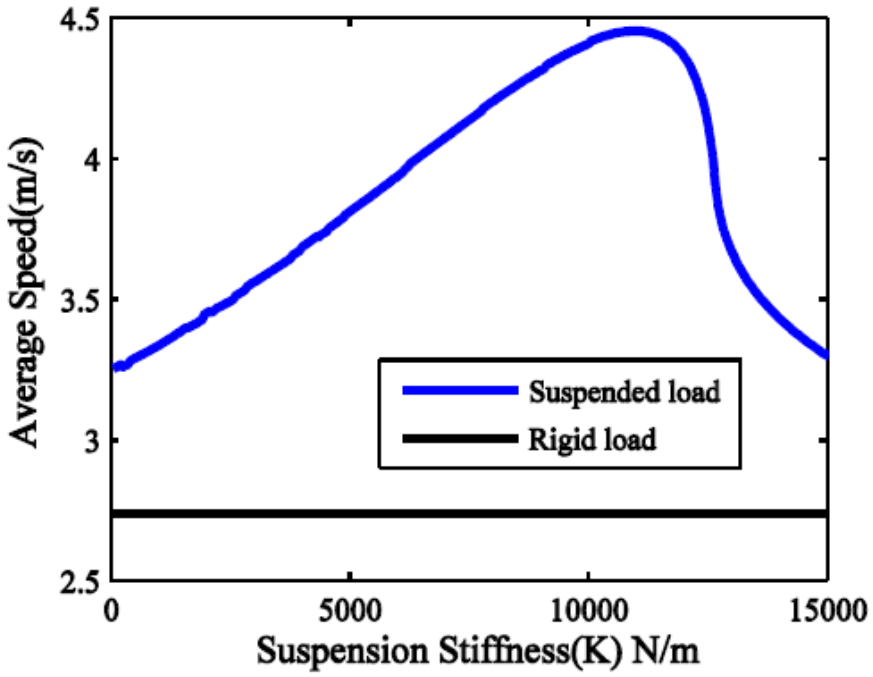

Figure 4.3. Average Speed Variation Due to Change in Suspension Stiffness.

4.2.3 Effect of Coupled Dynamics Portrayed by the System

The model shows that the amplitude of the body mass is reduced for suspended loads versus a rigidly-attached load during human running Figure 4.6, which could have a significant effect on the biomechanics of human running. The amplitude of the body mass is minimized when the natural frequency of the load suspension is tuned just below the resonant condition. The model also shows that the amplitude of the load mass is minimized as the load suspension stiffness is minimized Figure 4.5. The load suspension essentially acts like a vibration isolator. As expected, the amplitude of the load mass is maximized when the natural frequency of the load suspension is tuned near resonance.

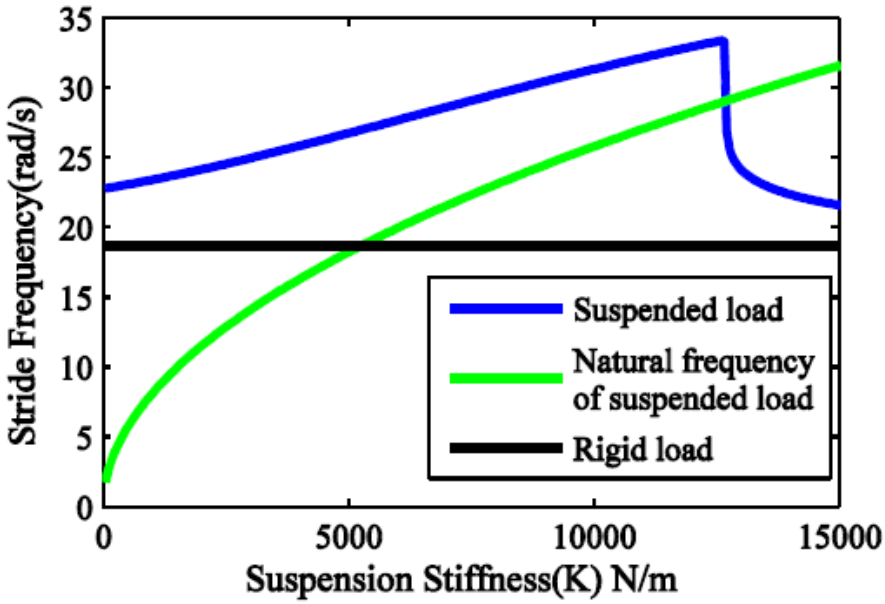

Figure 4.4. Change in Stride Frequency Upon Change in Suspension Stiffness.

4.2.4 Energetics and Peak Forces of the System

As with prior modeling work of a human walking with a suspended load [4, 6, 20, 27, 29, 30] the double mass model predicts that the peak forces of the load mass acting on the human body mass are reduced for suspension stiffness values below some critical stiffness K value Figure 4.7. The minimum peak force of 210 N acting on the body occurred when the load suspension stiffness K was minimized. As the suspension stiffness values increased, the peak forces of the load mass acting on the body mass continued to increase to 810 N until the load suspension stiffness was tuned near resonance. Beyond resonance, the peak forces decreased and approached the rigid condition.

The model shows that average power input during the stance phase per stride is greater with an elastically-suspended load than with a rigidly-attached load Figure 4.8. This suggests that the energetic cost of running with an elastically-suspended

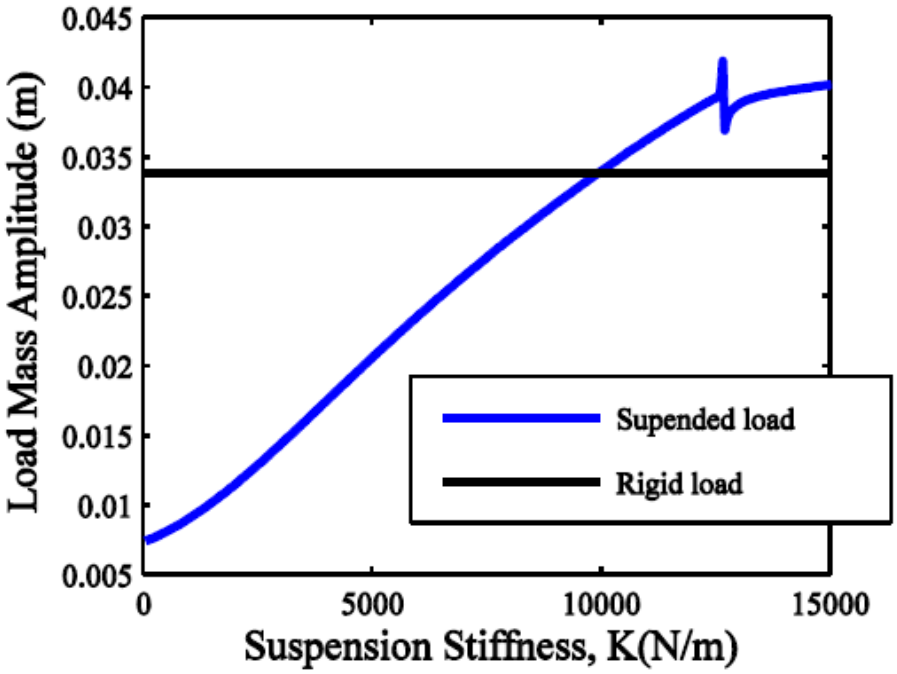

Figure 4.5. Variation in Load Amplitude Upon Varying Stiffness.

load is greater than running with a rigidly-attached load even though the peak forces acting on the body are reduced. This result differs from prior modeling work with the linear double-mass hopping model which shows that elastically-suspended loads may reduce the energetic cost of locomotion at lower walking speeds and frequencies [6]. However, the linear double-mass hopping model is likely only representative of human walking rather than running. Since the double mass Actuated SLIP model offers a better representation of human running, it likely provides a more realistic approximation of the energetic cost of running.

4.3 Discussion

A double mass Actuated SLIP model was developed to investigate the effect of elastically-suspended loads on the dynamics, forces, and energetic cost of human

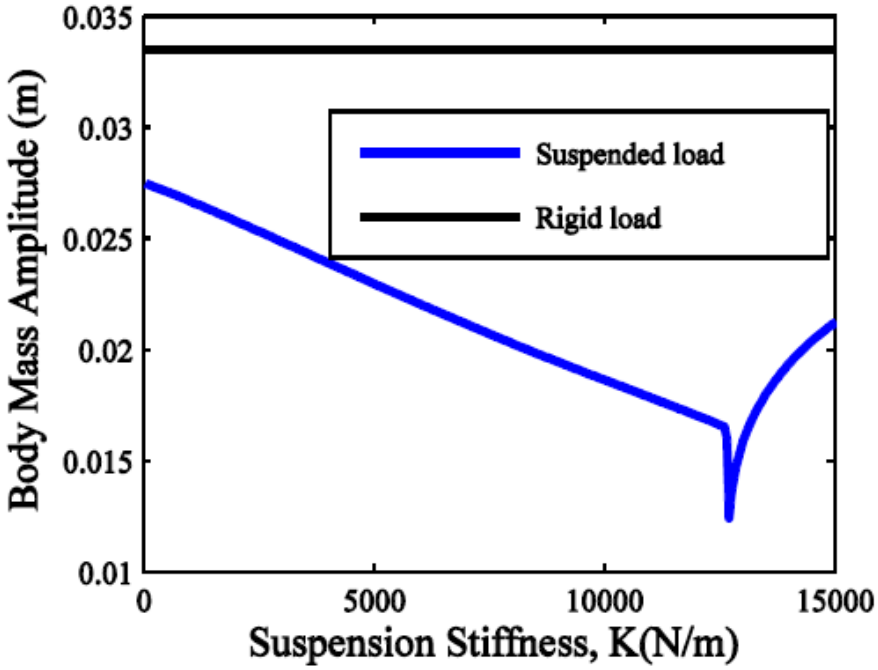

Figure 4.6. Variation in Body Amplitude Upon Varying Stiffness.

running. This model is a hybrid nonlinear system because it exhibits separate flight and stance phases that are governed by different equations of motion. Since human walking does not exhibit a flight phase, this model is not likely to be representative of human walking.

Although the double mass Actuated SLIP model may be representative of human running, it is important to note the limitations of the model. A major difference between this model and actual human running is the effective torque acting at the hip. At running speeds, the hip torque is about 40-80 N/m, the knee torque is about 125-273 N/m, and the ankle is about 180-240 N/m. All these torques occur during different parts of the stance phase [11]. The hip torque is dominant during the 1st half of stance and the ankle torque is dominant during the 2nd half of stance. As our model has a single effective spring-leg actuated by a torque about the hip/body mass, we averaged out the values of torque to a constant value. Since the reported

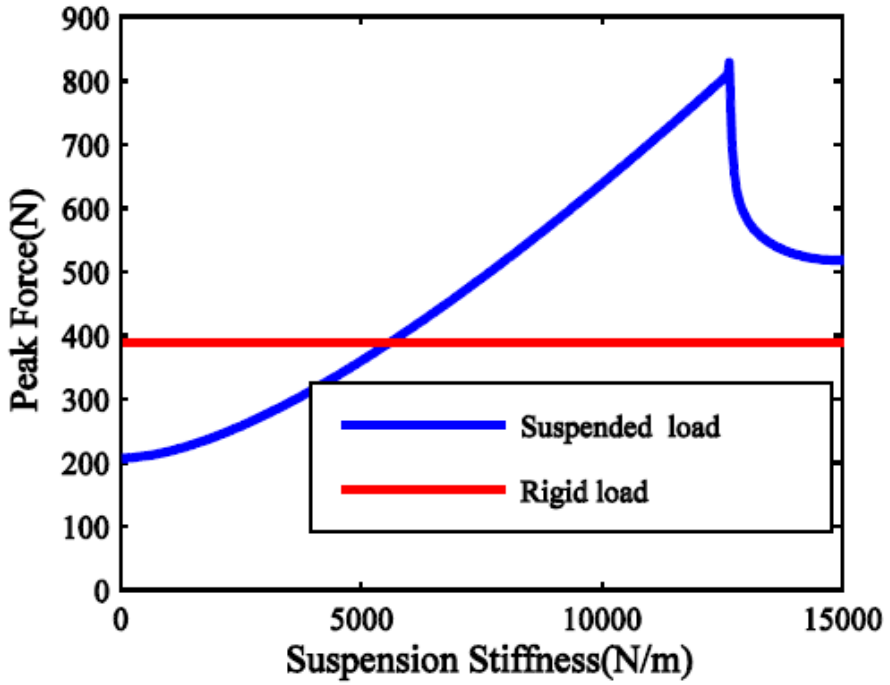

Figure 4.7. Plot Showing Trend of Maximum Force Experienced by the Body Mass Due to the Load Mass.

values were for a human running without a load, we increased our approximation of the average effective torque required for human running to $\tau = 300$ N-m because we expect that the torques would increase while carrying a 15 kg at the same speed. The effective torque of the effective spring-leg may also vary depending on the load suspension parameters. We chose this simplified approximation of the human leg to simplify the model for analysis. A better model of the effective torque and the dynamics of the human leg would more accurately capture the dynamics of running, but this approach may significantly increase the complexity of the model.

The running speed of the model is dependent on the leg torque, which is assumed to act only about the hip with a constant value throughout the stride. The model shows that the average horizontal speed of the body mass while running with a rigidly-attached load is approximately 2.8 m/s (or about 6.3 mph), which is a relatively

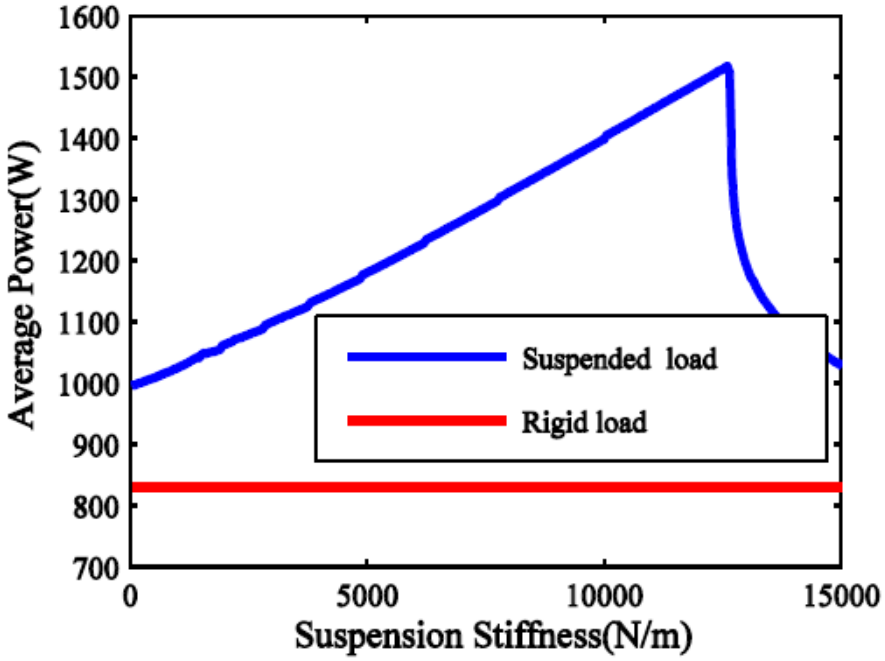

Figure 4.8. Variation in Average Power Upon Varying Stiffness.

fast-paced run while carrying a 15 kg load. As the load suspension stiffness is tuned near resonance, the average speed of running is increased to its maximum value of approximately 4.2 m/s, which may not be a realistic speed for a human to run while carrying a 15 kg load. We expect that the biomechanics of the human body would likely compensate in some way to avoid the resonant condition of running with a suspended load tuned near resonance.

The resonant stiffness of an elastically-suspended load occurs at a higher value than expected based on prior work with a double mass hopper model [6]. The stride frequency of the double mass Actuated SLIP model tends to increase as the natural frequency of the load suspension is increased until the resonant condition is achieved. The coupled dynamics of the load mass and the body mass appear to increase the stride frequency. Therefore, the resonant condition where the suspension stiffness K matches the stride frequency occurs at a higher value than expected. This coupling

between stride frequency and the load natural frequency would likely require significant bio mechanical changes to occur for a human to run at a constant speed while carrying a suspended load. A controller may be required for the double mass Actuated SLIP model to fix the average speed while the load suspension parameters are varied, which would be more realistic of a human running with a load at a constant speed (on a treadmill, for instance).

When making comparisons between human running with an elastically-suspended load versus a rigidly-attached load, it is important to determine how a rigidly-attached load is defined. One may define a load with a perfectly rigid attachment as a single lumped mass (m + M). However, a single lumped mass model has one less degree of freedom than the double mass model and would prevent analysis of the dynamic forces of the load mass acting on the body mass while running. We chose a conservative estimate of a rigidly-attached load through comparison with a single lumped mass model. However, a load cannot be attached to the human body with a perfectly rigid connection. The mechanical linkage between the load and the human body and the biomechanics of the human body while running can change the effective suspension stiffness and damping of a rigidly-attached load. Further work is needed to determine the actual parameters of a rigidly-attached load for human running.

The model shows that the amplitude of the body mass is reduced for low load suspension stiffness values compared to a rigidly-attached load during human running Figure 4.6. This would likely result in changes to the biomechanics of running with a load. The amplitude of the body mass is minimized when the natural frequency of the load suspension is tuned just below the resonant condition. The model also shows that the amplitude of the load mass is minimized as the load suspension stiffness is minimized, similar to a vibration isolator Figure 4.5. As expected, the amplitude of the load mass is maximized when the natural frequency of the load suspension is tuned at resonance. When the load mass is tuned near resonance, the load will exhibit a high amplitude of oscillation and the body mass will exhibit a minimum

oscillation at the anti-resonant condition. This phenomenon is similar to that of a tuned vibration absorber.

The model shows that the peak forces of the load mass acting on the body mass are reduced for an elastically-suspended load compared with a rigidly-attached load below some critical suspension stiffness Figure 4.7. The minimum peak force of 210 N acting on the body mass occurred when the load suspension stiffness K was minimized. It is important to note that the peak force of the load mass acting on the body mass will not be lower than the static force of the load mass M*g, or approximately 150 N. Therefore, it may also be helpful to examine the amplitude of the dynamic force acting about this static load force. At higher stiffness values, the peak forces of the load mass acting on the body mass continues to increase to 810 N until the load suspension stiffness was tuned near resonance. Beyond resonance, the peak forces decreased and approach the rigidly-attached load condition. This result is similar to prior work of human walking with a suspended load [4, 6, 20, 27, 29, 30], except that the resonant peak was shifted to higher suspension stiffness values than expected due to the coupling of the stride frequency and natural frequency of the load suspension. The load force is also dependent on the load suspension damping B value. The peak forces acting on the body tend to be minimized as the load suspension stiffness K and damping B are minimized.

The model shows that the energetic cost of running with a suspended load is increased compared to a rigidly-attached load Figure 4.8. However, Kram reported no measurable differences in the energetic cost of running while carrying a load with compliant bamboo poles versus a standard backpack [4]. It is unclear why this discrepancy between the experimental evidence and the result from our model occurred. The energetic comparison between a suspended load and a rigidly-attached load may depend on how a rigidly-attached load is defined. In this paper, we used a conservative estimate of a rigidly-attached load by comparing it to a single-lumped mass model, choosing very large suspension stiffness and damping values. As shown by Foissac et al. [29], an actual backpack could have considerably lower suspension stiff-

ness and damping values. Further modeling and experimental validation is needed to determine the effect of running with a suspended load on the energetic cost of running.

Both the peak forces and the energetic cost of running with a suspended load are maximized when the load suspension is tuned near the resonant suspension stiffness. Since tuning a suspended load near resonance may be desirable if the goal is to harvest energy from the motion of the pack, it is important to note that the peak forces and the energetic cost of human running may be maximized at resonance, which may not be desirable from a biomechanics perspective.

The results of the model qualitatively confirm the experimental work on human running with elastically-suspended loads by Rome et al. [27] and Kram [4], showing that walking with an elastically-suspended load is different than running with one. These differences between walking and running are likely a result of the coupled non-linear dynamics introduced by the flight phases during human running. This work could enable a more complete understanding of human locomotion with elastically-suspended loads and lead to the design of load suspension systems that can minimize stress on the human body.

In this paper, we focused on the effects of the load suspension stiffness K. To fully understand the effect of a suspended load on human running, a larger parameter study should be performed, particularly to investigate the effect of the load suspension damping B and the load mass M. The load suspension damping is likely a critical parameter of the system. Low suspension damping may be desirable, but could present certain trade offs. The effect of the load mass M is not presently known. Given that humans run with a wide range of loads, such as school children running with light backpack loads to some soldiers running with a load up to 50-80% of their own bodyweight, understanding the effect of the load mass could be important.

5. ASSESSING THE STABILITY OF THE DOUBLE MASS HIP-SLIP

Humans carry out their movement from one point to the other through locomotion which can be either walking or running [12]. In doing so we vary our speed depending on the time we need to spend from moving between the two places. At a given speed a person can either run or walk. The the transition from walking to running depends on the stability as well as the ease with which the human can run [31]. If the gait is not well suited to move, it will lead to imbalance. Instability among humans is caused by either slip, trip or fall and in most cases an external agent causes this events to occur. Walking and running with a load is expected to be a difficult task as there certain changes to the body posture and leg movements. To study the stability in human locomotion while carrying heavy loads we need to perform a stability analysis.

As Shen et.al. showed in his paper, the single mass actuated SLIP predicts better stability when compared to a conservative SLIP model [7]. A leg damper is effective in dissipating energy produced by the hip torque as well as absorbing external forces which are encountered by the system due to perturbations. The nature of stability in a double mass Hip-SLIP model will be different as compared to a single mass model, due to the addition of two more states defining the position and velocity of the load mass. Previous studies on a double mass hopper model by Ackerman et al. show that locomotion with elastically suspended loads tend to have less stability as compared to rigidly attached loads [30]. Though those results were based on a suspended load on a hexapod robot, it would be fair to say that elastically suspended loads can decrease the stability of the system.

5.1 Human and Suspension Parameters

The human parameters used in this study are almost similar to those used in the previous chapter on energetics of human running. The average human mass in this analysis was considered as 70 kg. The parameters used are mentioned in Table 5.1. The suspension stiffness is varied between 50 to 15000 N/m while the suspension damping is varied between 10-100 Ns/m. Varying the suspension parameters to test the stability of the system will give us a fair idea of as to how the model stability changes for low to high stiffness values.

Table 5.1.
Human Lower Body Parameters.

Parameter	Value
Leg Stiffness, k	14500 N/m
Leg Damping, c	950 Ns/m
Leg Angle, β	65^o
Hip Torque, τ	250 Nm
Body Mass, m	70 kg

5.2 Evaluating the Fixed Points

The Double Mass Hip-SLIP will have four state parameters as opposed to two in the actuated SLIP [7]. In order to evaluate the stability of the system the model needs to propagate with periodic motion. This periodic gait acts as a prerequisite to assess the stability of the system. To evaluate the fixed point the model is given a set of initial conditions $IC = [v, \delta, y_u, \dot{y_u}]$, which are allowed to converge to a set of final conditions which act as the fixed points for that parameter set $FP = [v_o, \delta_o, y_{uo}, \ddot{y_{uo}}]$. The set of values defined by FP will make the system run at a

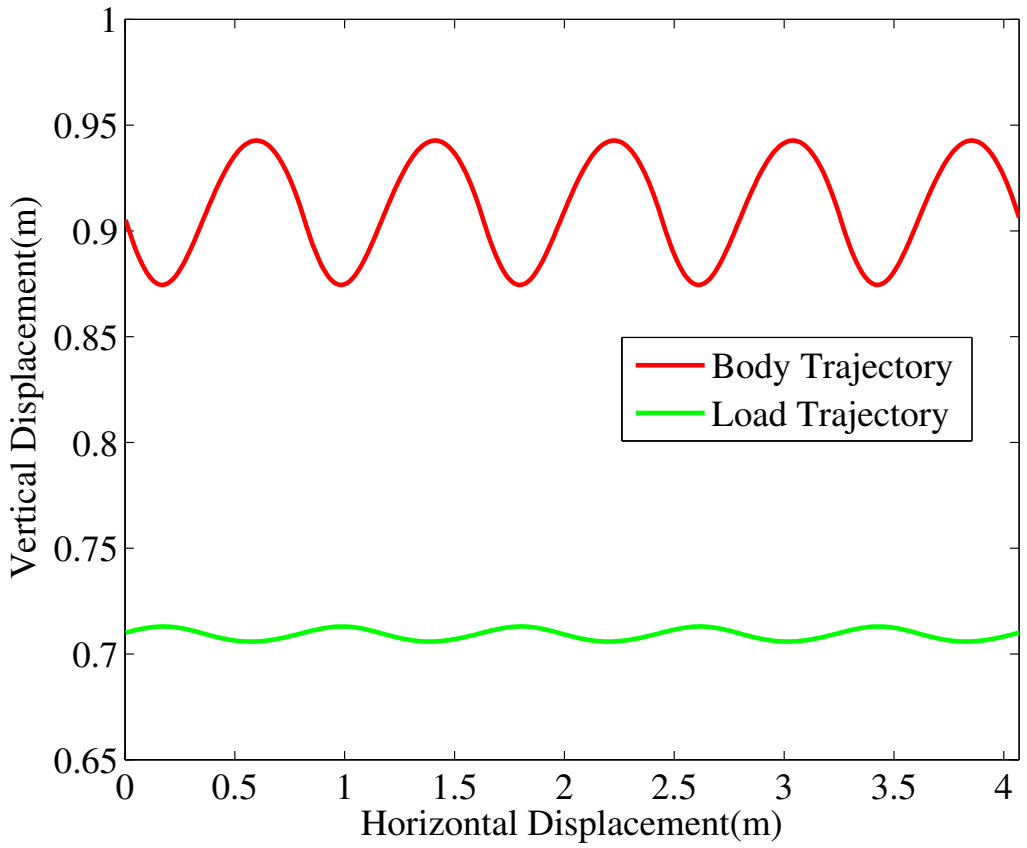

Figure 5.1. Fixed Point Trajectory at the Human Parameters Specified in Table 5.1 with K=500 and B = 25 Ns/m.

constant periodic trajectory with a fixed/unfixed amplitude of load and body. For example using parameters from Table 5.1 and at K=500, B = 25 Ns/m the fixed points come out to be $FP = [2.8852, 18.7113, 0.7101, 0.0712]$. The trajectory of this fixed point set is shown in Figure 5.1.

5.2.1 Multiple Period Fixed Points

Some fixed points may deviate from portraying single period to displaying more than one period. In such a multiple period system the trajectory of the model repeats

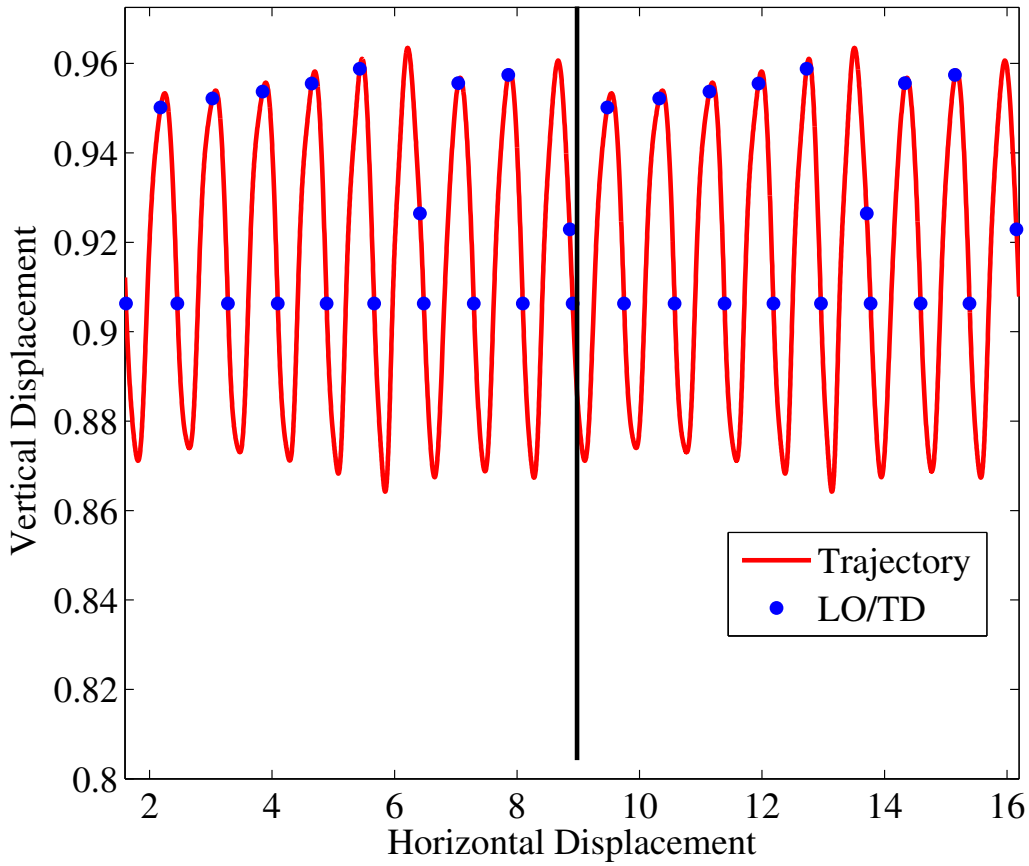

Figure 5.2. A Period 9 Trajectory Portrayed by the Double Mass Hip-SLIP.

after every n_{th} lift off condition. The touch down conditions occur after every one cycle but the lift off condition value set repeats after every n_{th} cycle. The number of stride periods that can occur before a trajectory repeats can become very large. Sometimes the model depicts uncertain periodicity, with no constant period. For such a behavior there is not a definite period value and establishing a constant pattern of the trajectory is difficult.

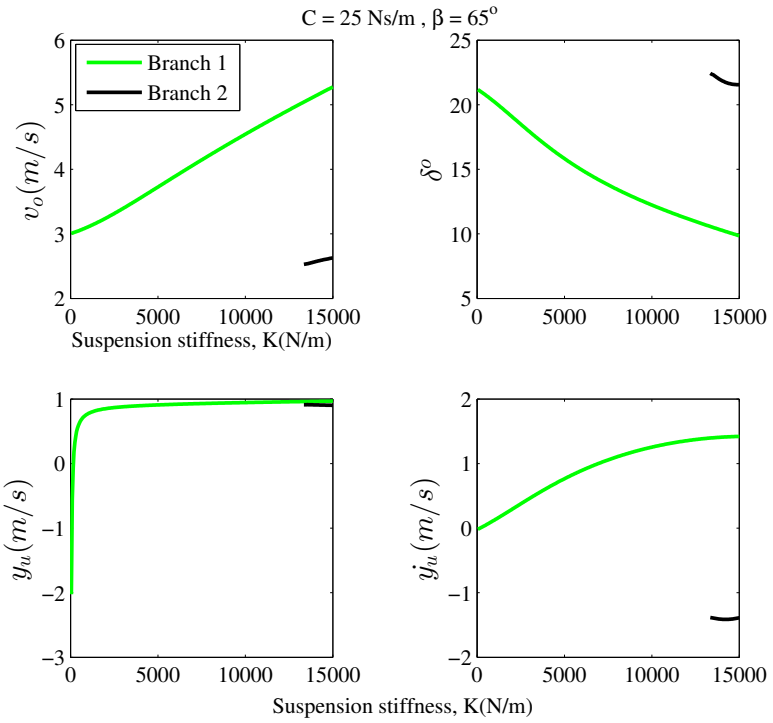

Figure 5.3. Branching Occurring in for the Human Parameters Mentioned 5.1 and at B= 25 Ns/m as Stiffness is Varied.

5.3 Branching in Fixed Points

In order to observe the trend in the state variables of the system we varied the suspension stiffness. For every set of parameters we get a unique set of fixed points. These fixed points can either be a part of a common curve showing continuity or they can break away from the current curve and branch out into a separate curve. In the Figure 5.3 we observe the primary curve discontinuing at K=13650 N/m.

5.4 Eigenvalue Analysis

Eigenvalue analysis is a linearized method of assessing the stability of a model. The fixed points evaluated in the section above can either be stable or unstable.

The branches in fixed points can both be stable, both unstable or only one of them stable. To evaluate the stability we measure the effect of disturbances in the system during it's periodic gait. In this case the system while propagating at a constant periodic trajectory, is provided with a certain perturbation of magnitude 0.01 to the fixed point values in succession at touch down. The disturbance remaining in each of the state parameters is noted at the next touch down. To evaluate the effect of these perturbations we construct a Jacobian which is a nxn return map. The initial condition $FP = [v_o, \delta_o, y_{uo}, \dot{y}_{uo}]$ of the system is perturbed and noting the difference at the successive condition either lift off or touch down using finite differences, the matrix is constructed. Δv, $\Delta\delta$, Δy_u and $\Delta\dot{y}_u$ are the errors in velocity, δ, load displacement and load velocity respectively. While, Δv_p, $\Delta\delta_p$, Δy_{up} and $\Delta\dot{y}_{up}$ are the magnitudes of perturbation provided to the system

$$J_{4X4} = \begin{Bmatrix} \frac{\Delta v}{\Delta v_p} & \frac{\Delta v}{\Delta \delta_p} & \frac{\Delta v}{\Delta y_{up}} & \frac{\Delta v}{\Delta \dot{y}_{up}} \\ \frac{\Delta \delta}{\Delta v_p} & \frac{\Delta \delta}{\Delta \delta_p} & \frac{\Delta \delta}{\Delta y_{up}} & \frac{\Delta \delta}{\Delta \dot{y}_{up}} \\ \frac{\Delta y_u}{\Delta v_p} & \frac{\Delta y_u}{\Delta \delta_p} & \frac{\Delta y_u}{\Delta y_{up}} & \frac{\Delta y_u}{\Delta \dot{y}_{up}} \\ \frac{\Delta \dot{y}_u}{\Delta v_p} & \frac{\Delta \dot{y}_u}{\Delta \delta_p} & \frac{\Delta \dot{y}_u}{\Delta y_{up}} & \frac{\Delta \dot{y}_u}{\Delta \dot{y}_{up}} \end{Bmatrix}$$

5.4.1 Estimating the Torque Value

From Chapter 2 we see that a three-link leg model consisting of hip, leg and ankle can be reduced to a single link model under the assumption that all the links are massless. The torques are lumped as an effective hip torque. To further investigate the magnitude of torque used, a stability analysis was performed on a single mass actuated SLIP model with human parameters as mentioned in Table 4.1 with the center of mass being = 85(body+load) kg. This was done so as to make the model behave like a rigid system having both the human and load masses.

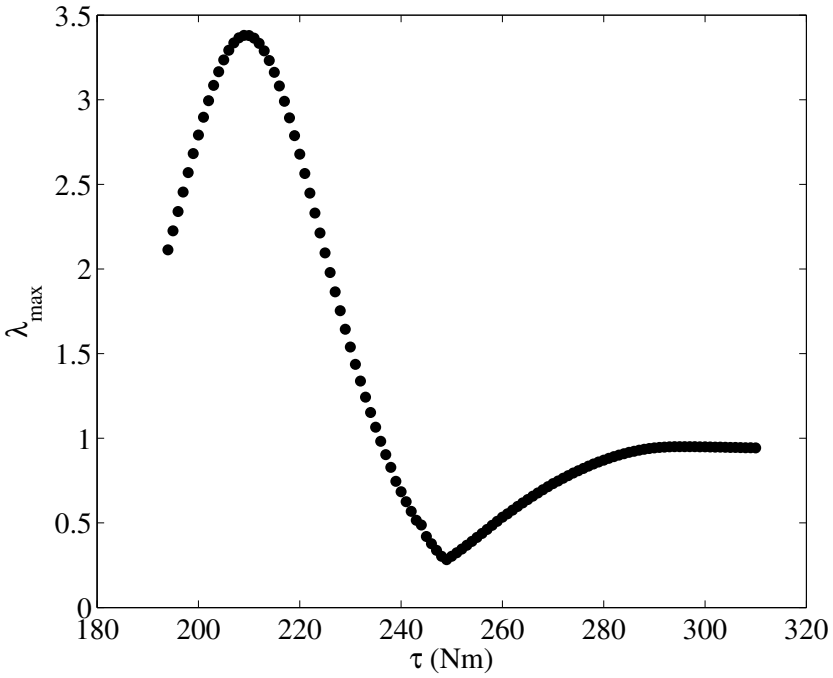

Figure 5.4. Eigenvalue of Single Mass Actuated SLIP for Different Torque Values.

Figure 5.4 shows that the single mass system is most stable at τ=250 Nm. This single mass system becomes unstable towards lower torque values. For a torque below 192 Nm and a fixed torque value was not found, thereby implying the system does not have a periodic gait for these parameter values. For torque larger than 315 Nm the system was not able to synchronize it's flight and stance phases and crashed before achieving steady state.

5.4.2 Stability of Suspended Load Hip SLIP Model

The steady increase in the center of mass velocity for the double mass system was a drawback of this system as humans carrying loads or running without loads can run at a constant forward speed. The occurrence of branches in the fixed points

showed that the model was capable of possessing two steady state parameter set. Such a trend was observed for all damping values of suspension. To characterize this phenomena occurring in the system , stability analysis by varying suspension stiffness was done.

Figure 5.5 shows the trend in the eigenvalues for both the branches. Eigenvalues in the vicinity of region show splitting into conjugate complex pairs. Throughout the stiffness regime two of the eigenvalues overlap except near a stiffness value of 2000 N/m. The system shows stability throughout the stiffness range for the first branch. Occurrence of high magnitudes of center of mass velocity in this branch are well within the stable range. For the second branch starting at approximately 13500 N/m the system shows instability. This feature can be attributed to the fact that branching occurs in the region of high instability as seen in the second branch eigenvalue plot.

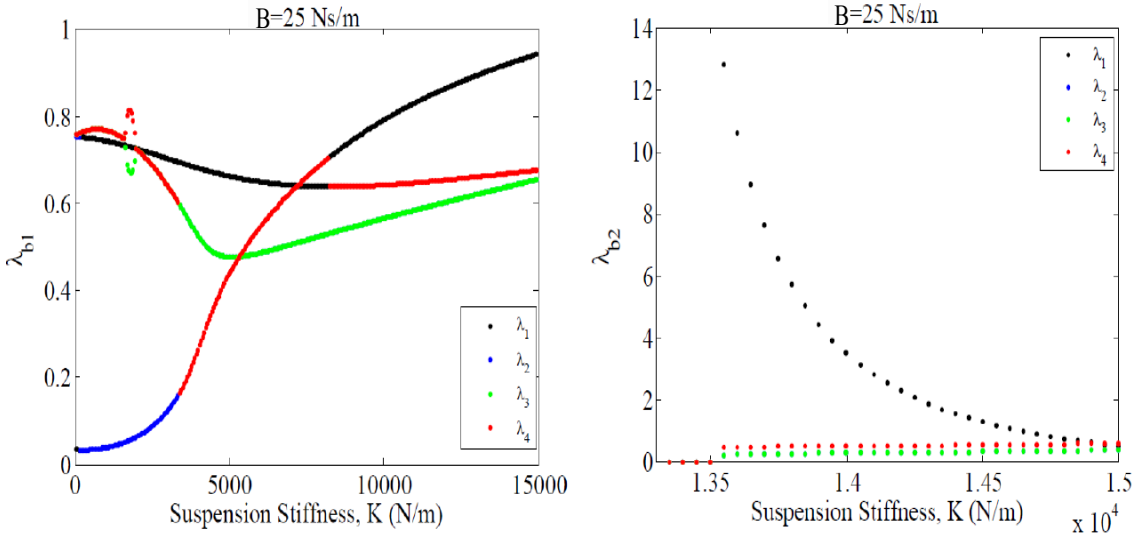

Figure 5.5. Eigenvalues at B=25 Ns/m with the Plot on the left Showing Eigenvalues for the first Branch and the on the Right Eigenvalues for the second Branch.

Considering the maximum eigenvalue trend in comparison to the previous plot, Figure 5.6(a) shows the overlapping of the maximum eigenvalue trends. Branch 1 is

stable while branch 2 approaches stability from the unstable region and gains stability as the stiffness is increased. Occurrence of two fixed points with one stable and the other unstable is characteristic of a saddle node bifurcation. Such a bifurcation can create, coalesce and destroy fixed points based on the constant parameters used [32]. The second branch showing instability within K = 13500 N/m to K= 14650 N/m shows the model prefers to move at a high velocity state but prefers a low velocity state from K = 14650N/m to K = 15000 N/m. As the damping value is increased to 50 Ns/m, branch 2 penetrates inwards and possesses fixed points for lower suspension values. Branch 2 shows a discontinuity in between as seen by the blue curve in Figure 5.6(b).

Eigenvalues for B=75 and 100 Ns/m show a somewhat similar trend. The discontinuity in the second branch at B=75 Ns/m and B= 100 Ns/m disappears as the damping value increases. The discontinuous region seen for B=50 Ns/m turns into a stable peak for B=75 Ns/m as seen in Figure 5.7(a). This occurs due to more energy dissipation caused by increase in damping. As the damping value is increased to B=100 Ns/m the second branch gets even more stable as seen in Figure 5.7(b).

5.5 Attraction Basin between the Fixed Point Branches

To analyze the basins of attraction between the two branches of fixed points, the basin of attraction was plotted for each of the two fixed points. Figure 5.8 shows the region between the two branches. The region colored in pink shows affinity towards the first branch while the region in gray show affinity towards the second branch. The stiffness at which the second branch starts has a narrow grey region signifying the parameter space is more attracted towards the first branch. As we move towards stiffer values the affinity of the second branch increases as opposed to that of the first branch. The line separating the two regions of the parameter space acts as separatrix which contains points attracted towards neither of the branch.

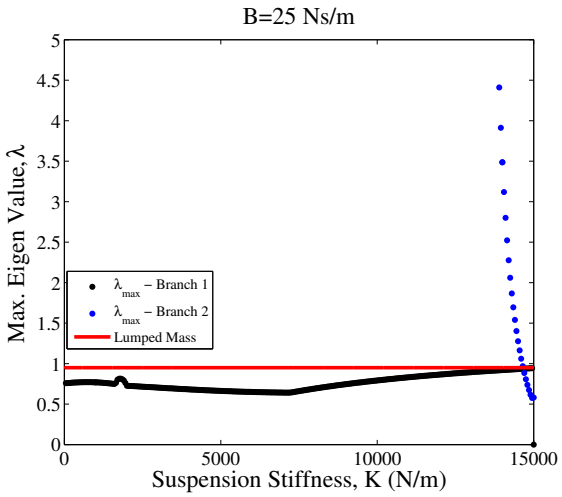

(a) Maximum Eigenvalue at B=25 Ns/m.

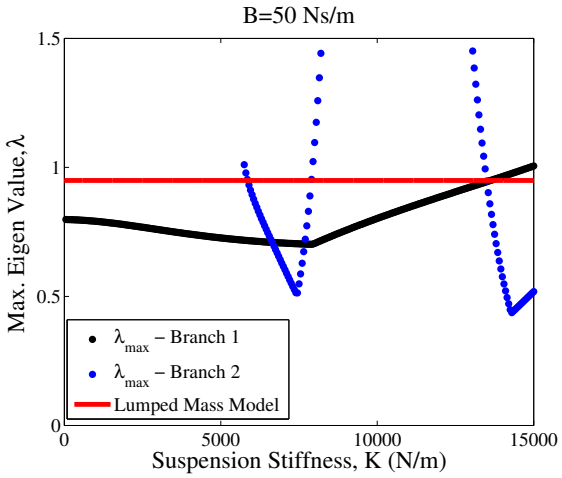

(b) Maximum Eigenvalue at B=50 Ns/m.

Figure 5.6. Maximum Eigenvalue Trend at B=25 & 50 Ns/m.

Figure 5.9 shows the magnified view of the region in between the two branches. This method of measuring the attraction of the branches works on minimization of error. Starting with a set of initial conditions, the system over a period of N cycles achieves a fixed point, which can either lie on the first or the second branch. A similar analysis is done on an actuated SLIP constant torque model by Shen et al. [7].

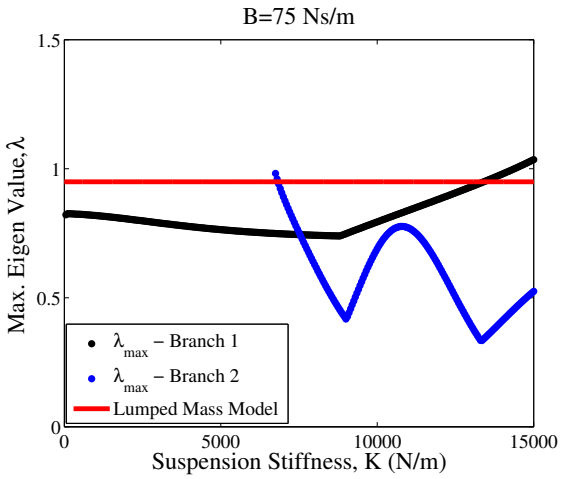

(a) Maximum Eigenvalue at B=75 Ns/m.

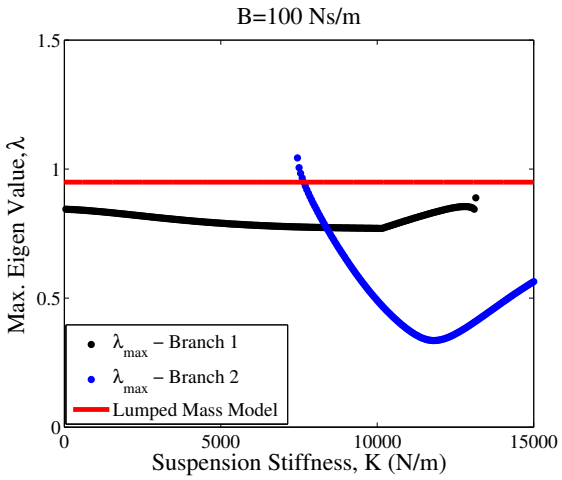

(b) Maximum Eigenvalue at B=100 Ns/m.

Figure 5.7. Maximum Eigenvalue Trend at B=75 & 100 Ns/m.

5.6 Discussion

Fixed points for the Hip Actuated model show branching for all the damping values of the suspension. This occurrence of branches could be an outcome of the coupled mass dynamics that occur for this hybrid system. The system is an open loop non linear system without control over any of the parameters except for leg placement during the flight phase of motion. A slight variation in the parameter can shift the

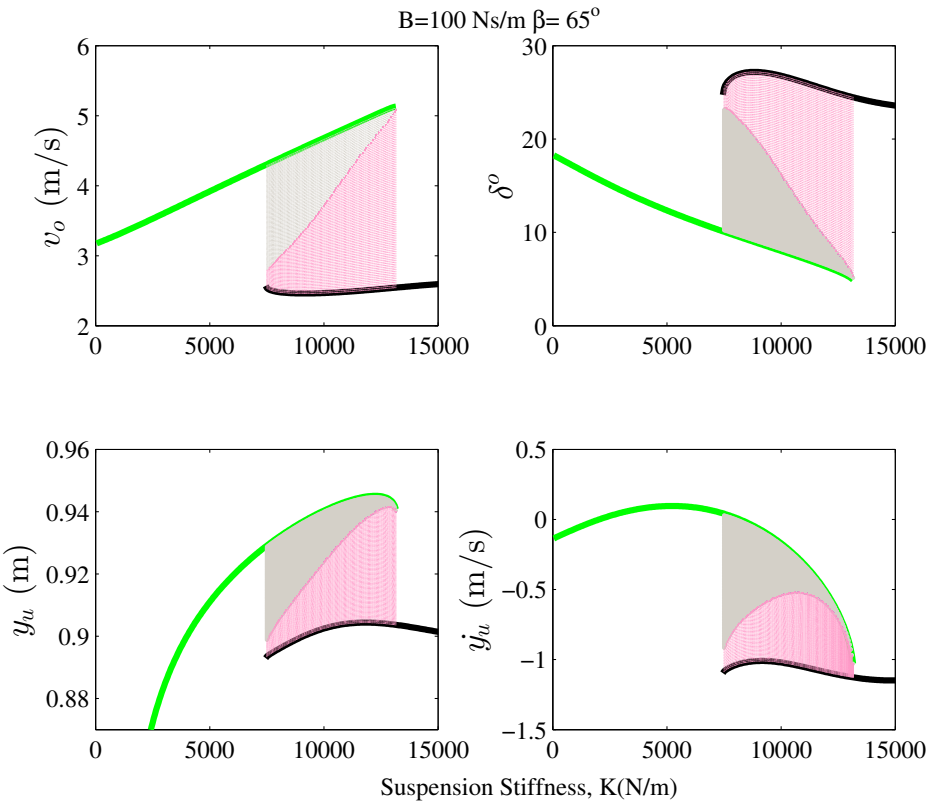

Figure 5.8. The Pink Region Encloses the Points Which are Attracted towards the Black Branch while the Grey Region Encloses Points Attracted to the Green Branch .

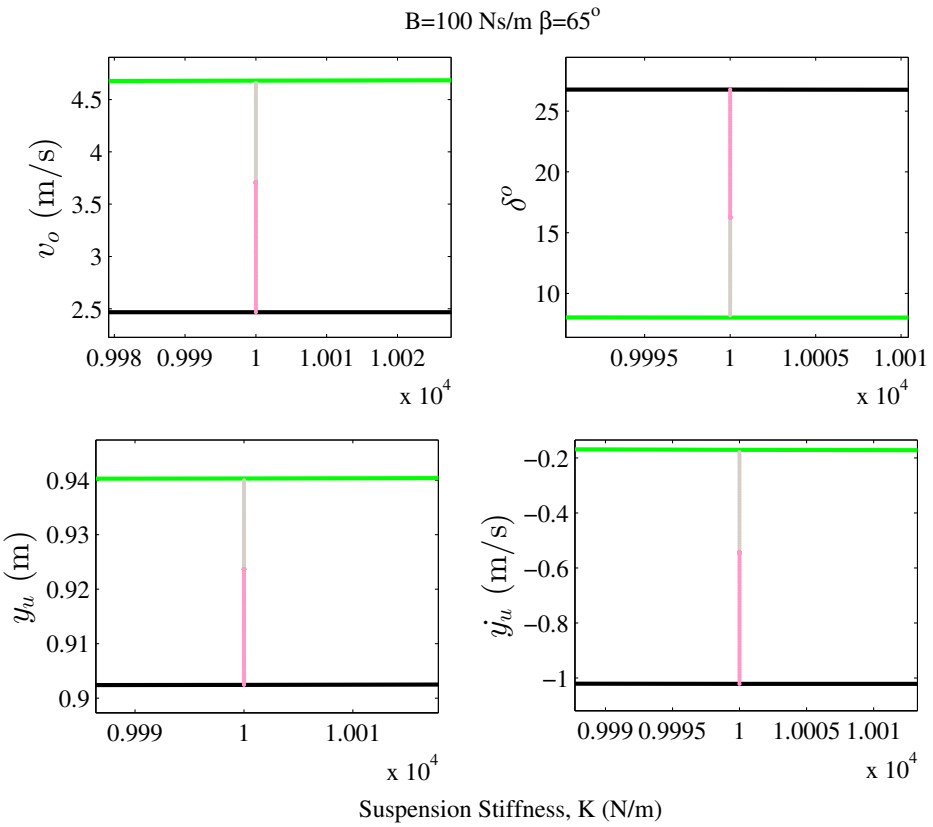

Figure 5.9. Sink Showing the Narrow Region Between Two Fixed Points at a Given Suspension Stiffness.

system to a new steady state. As the suspension stiffness increases, the velocity of the center of mass increases.

The model also shows multiple periodicity for a few parameter sets. Multiple period systems are mainly characterized by increase in body amplitude with irregular lift off conditions. Previous studies on a an actuated SLIP Model [7] with a single mass show fixed points with period 1 trend.

Jacobian represents a linearized version of the stride map. It provides a fair assessment of the stability of fixed points. Among all the eigenvalues the maximum eigenvalue defines the time scale of response to perturbations of the system. The system shows stability for a large forward velocity which might be unrealistic while

carrying a heavy load. As the damping of this system is increased, the second branch shows high stability due to high energy dissipation as seen in the blue curve in Figures 5.6(b), 5.7(a), 5.7(b) for B=50, 75, 100 Ns/m respectively. This shows that for high energy dissipation the model achieves more stability.

6. VELOCITY CONTROLLED HIP ACTUATED SLIP MODEL

Human gait depends on multiple parameters. A human running or walking at constant speed will have a set of system parameters appropriate for that gait. An addition of load will change the dynamics of the system due to the coupling that occurs between the load and the body. This can be seen in the constant torque model which is not able to contain it's velocity at a given value. The velocity and stride frequency increase as the suspension stiffness is increased [24]. This drawback is due to the fact that there is no feedback in the constant torque model. This leads to uncontrolled stride frequency and forward velocity. For a given set of parameters the model settles to a particular stable periodic solution and sometimes attains unrealistic speeds which are not possible for a human to attain while carrying heavy loads. Kram showed that in order to maintain a constant velocity while carrying loads on springy poles, the aerial time decreases compared to running without the poles with the same horizontal speed [4]. This in turn changes the stride frequency and stride length of the person. In order to accommodate for the change in the stride frequency and stride length, a human adjusts his or her leg landing angle. This altering of gait due to a load modifies the dynamics of the constant torque model.

6.1 Comparing System Kinematics of the Two Models

To reduce the variation in speed and stride frequency while keeping the leg angle constant, we developed a velocity control model as mentioned in Chapter 3. Instead of a constant hip torque, the hip torque varies to achieve the target constant velocity. We designed a controller for a set of system parameters used by Kram in his experiment on springy poles. Table 6.1 specifies the leg stiffness, leg damping and leg angle. The constant torque model was given a torque of $\tau = 250Ns/m$ which was used in the

previous chapter on stability analysis, while the velocity control model was given a gain g_τ of 1100 Ns. This was a suitable gain value as the RMS value of the torque during the stance time was almost 250 Nm. In order to compare the velocity w.r.t. the suspension stiffness fixed points were calculated for each stiffness value. The horizontal velocity fixed point was then plotted against the corresponding stiffness value. This plot provides a good measure of the change in forward velocity of this velocity controlled model. The variable torque attains a maximum value of 440 Nm

Table 6.1.

System Parameters.

Parameter	Value
Leg Stiffness, k	14500 N/m
Leg Damping, c	950 Ns/m
Human Mass, m	78.8 kg
Leg Landing Angle , β	65^{o}.
Load Mass, M	15 kg
Suspension Damping, B	1.77 Ns/m

during the stance phase. The torque increases as the leg angle increases to 90 degrees and then subsides beyond 90 degrees. This torque profile resembles the hip torque profile as seen in Chapter 2 in Figure 2.2.

As seen in Figure 6.2 the change in horizontal speed of the velocity control model is minimum as compared to the constant torque model and is in close proximity to 3 m/s. Towards resonance when $\omega_{strd} = \omega_n$ the system becomes stiffer and sensitive to slight changes in the parameter value. This in turn causes discontinuity in the velocity trend due to amplification of oscillations in the resonance region. Similar to the velocity curve plot the stride frequencies of the two models have an analogous behavior to the velocity trend which can be seen from Figure 6.3. We used a suspension damping of

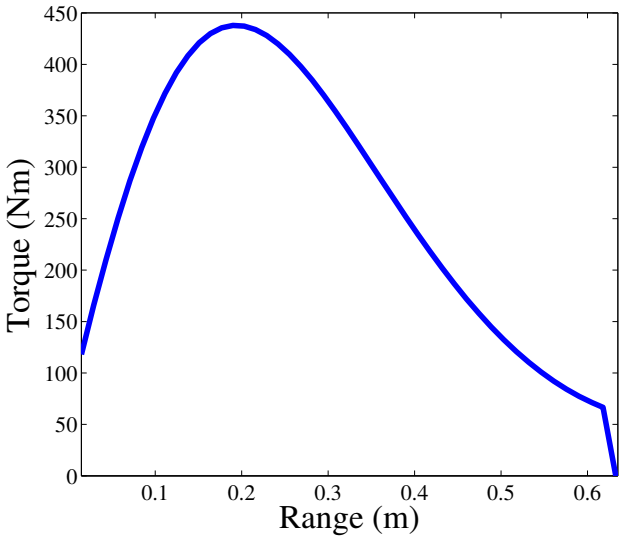

Figure 6.1. Torque Profile During the Stance Phase.

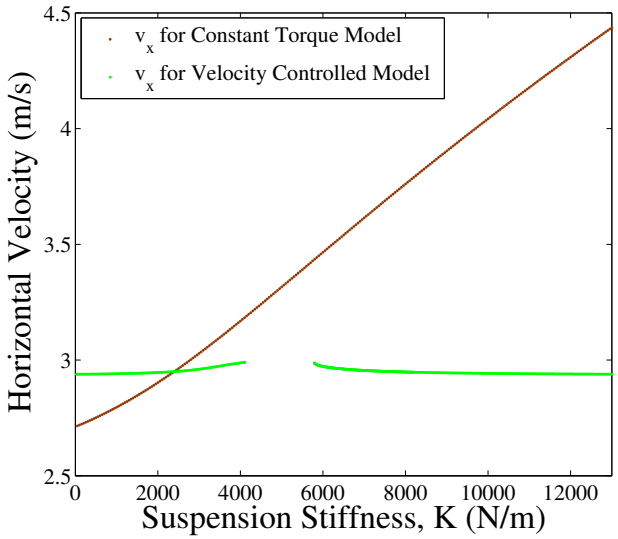

Figure 6.2. Change in Velocity of the Two Hip-Actuated SLIP Models.

$B = 1.77Ns/m$ as specified by Kram in order to plot the stride frequencies of both the models. The constant velocity model shows a discontinuity near resonance as

the stride frequency equals the damped natural frequency of the load. Due to the system being stiff and limitations of the MATLAB ODE solver, fixed points in the resonance region were hard to obtain. Kram evaluated the stride frequency with no load to be around 17.09 rad/s. The constant velocity model has a stride frequency of approximately 20 rad/s with an elastically suspended load. The increase in stride frequency occurs because the load pushes against the body causing decreased aerial time. But in order to maintain the same forward velocity the stride length shortens and thereby increases the stride frequency.

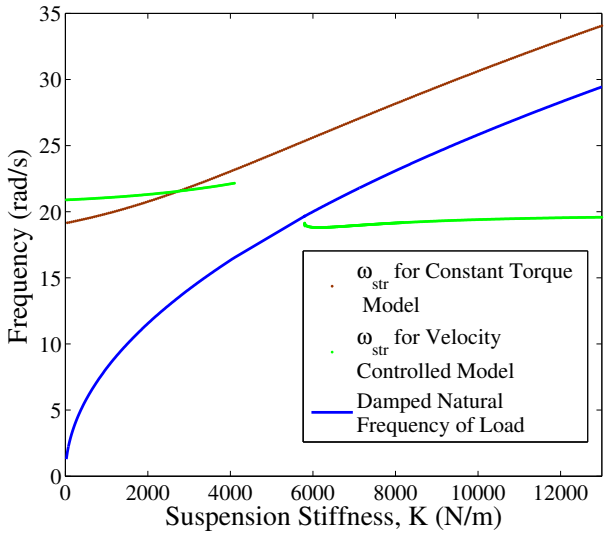

Figure 6.3. Comparison of the Stride Frequencies of the Two Models.

As the system approaches resonance the transmissibility increases thereby magnifying the amplitude of the load mass. This causes very high peak forces and in turn pushes the body against the ground. This increases the foot contact time and decreases the flight time of the person running. As discussed in the previous section the decrease in aerial time causes increase in stride frequency. This can be seen in Figure 6.4 with the lowest damping having the maximum stride frequency as it has least energy dissipation and high amplitude magnification. As we varied the damping

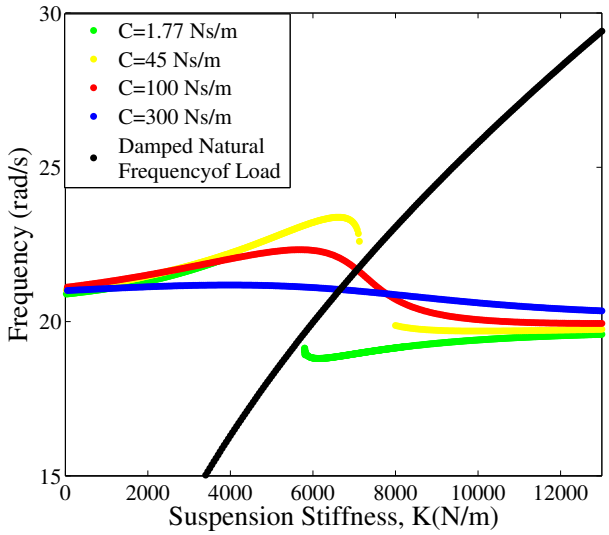

Figure 6.4. Variation in Stride Frequency Upon Varying Damping Constant.

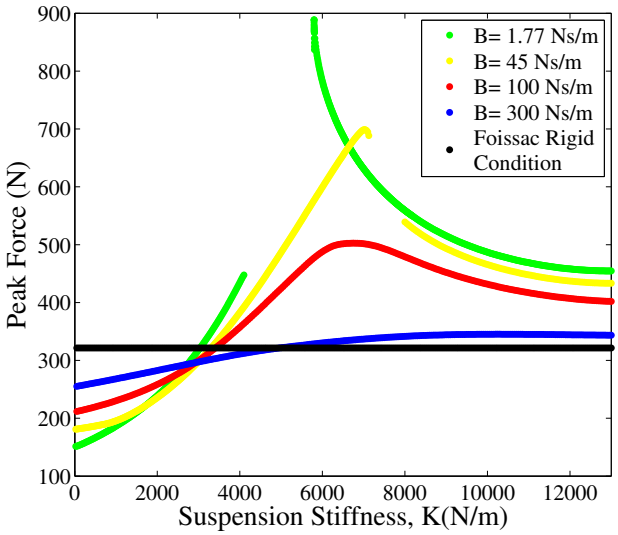

Figure 6.5. Change in Peak Force Trend Upon Increasing Damping Values.

of the suspension to higher values to observe the behavior of the model, the force trend showed striking resemblance to that of the peak force plot published by Hoover et al. Though Hoover published results on walking while carrying heavy load and this study deals with running, the similarity in the trend show that the behavior of the two types of locomotion with elastically suspended loads is similar in regards to the peak forces of the suspension on the body [20].

Figure 6.5 shows the peak force trend for various damping values. Resonance occurs when the input frequency equals the damped natural frequency of the load. Increasing damping values lower the resonance peak. Due to higher dissipation of energy there is a decrease in the amplitude of oscillations. At resonance low damping increases the magnitude of transmissibility. This increase in transmissibility causes the load to undergo high amplitude oscillations and increases sensitivity of the model to change in stiffness value. For very low stiffness value we get decoupling between the load and the body leading to the phenomena of vibration isolation. The slight shift in the peaks of the various curves is observed because of the error in the forward velocity. The velocity control model can restrict the velocity near the target velocity but not be equal to it. This causes the stride frequency to change and thereby shifts the resonance peak slightly. Foissac showed for a suspended backpack, rigid behavior is observed at a suspension stiffness of 5000 N/m and at a damping of 300 Ns/m [29]. We observed at a damping of 300 Ns/m the peak force asymptotically approaches the Foissac rigid line as seen in Figure 6.5. For very low stiffness values, the peak force decreases due to vibration isolation, making the load oscillate about the static value of 147 N.

6.2 Stability of the Velocity Controlled Model

Compared to the branching in fixed points seen in the constant torque model, the velocity control shows continuity in the fixed points, with the exception discontinuity that occurs at resonance where the equation becomes stiff and doesn't yield any

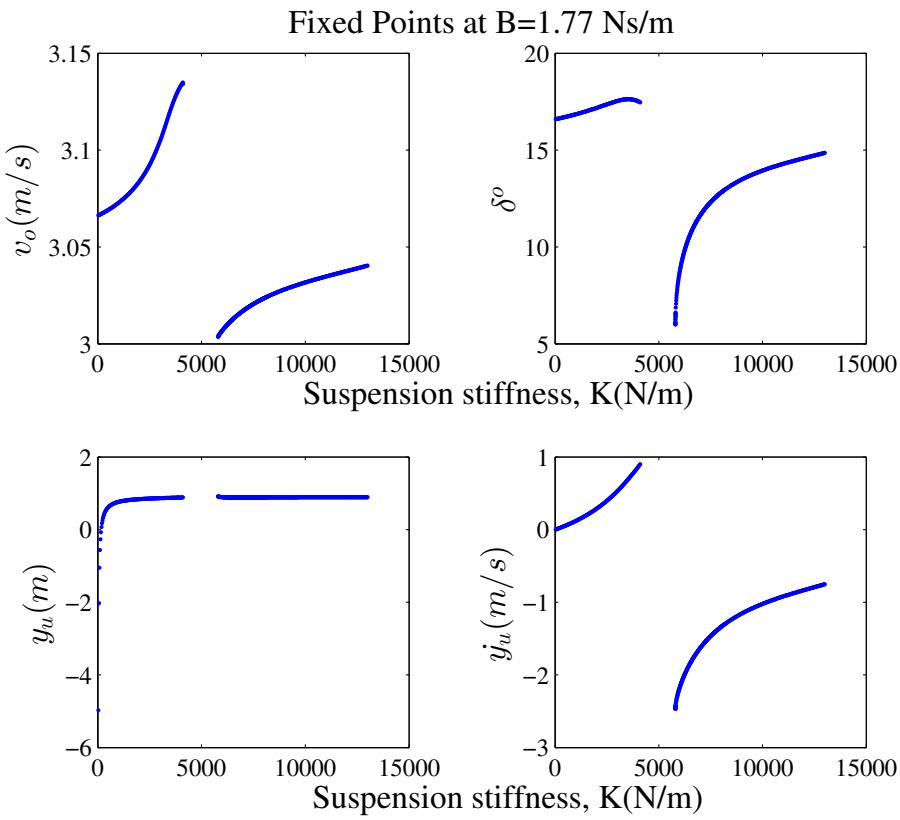

Figure 6.6. Fixed Points over Variation of Suspension Stiffness.

periodic solutions. Figure 6.6 shows the fixed points at B=1.77 Ns/m. Near resonance due to high amplification caused due to high transmissibility the load mass fixed point velocity increases in the vicinity of the resonance region. The forward velocity of the body is given by $v_x = v_o \cos \delta_o$. In order to compensate for the increase in the center of mass velocity δ increases, thereby keeping the forward velocity close to the target velocity. As seen in the Table 6.2 the center of mass velocity decreases as the damping constant is increased.

Table 6.2.
Fixed Points at K = 525 N/m.

Damping(Ns/m)	FP=$[v_o, \delta, y_u, \dot{y_u}]$
B = 1.77	$[3.069, 16.72^o, 0.62999, 0.05794]$
B = 45	$[3.067, 16.15^o, 0.634955, 0.027113]$
B = 100	$[3.063, 15.51^o, 0.652277, -0.04108]$
B = 300	$[3.048, 14.38^o, 0.62901, -0.31401]$

6.2.1 Eigenvalue Analysis

To evaluate the stability of this model we use the eigenvalue analysis as used in the previous chapter. We plot the maximum eigenvalues w.r.t. the suspension stiffness. Unlike the constant torque model, the fixed points for the velocity control model display no overlapping branches. From Figure 6.7 we observe that the model shows increased stability as the damping of the suspension is increased. This can be attributed to the fact that there is more energy dissipation which leads to rapid decaying of perturbations. Near resonance where the model becomes stiff and sensitive to small variations in stiffness values, the system becomes unstable.

Assessing the behavior of the eigenvalues at low stiffnesses, we observe a dip in the maximum eigenvalues towards achieving greater stability. This dip in the eigenvalue occurs for damping values of 45, 100 and 300 Ns/m, while for B = 1.77 Ns/m the system remains borderline stable. For systems with very low damping constant the system the system is not completely capable of decaying the perturbation. This insufficient decay of perturbation makes the system lie near the boundary separating stable and unstable regions. At B = 300 Ns/m unlike for B = 1.77 Ns/m, the system is more effective in decaying these perturbations.

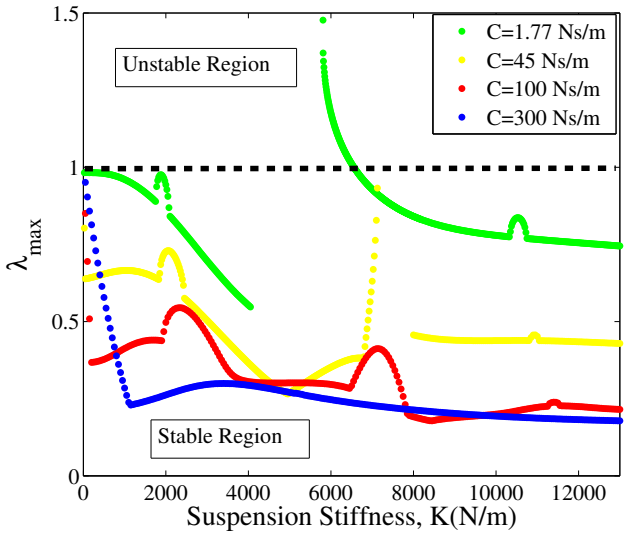

Figure 6.7. Eigenvalue Trend for the Model at Different Suspension Stiffness.

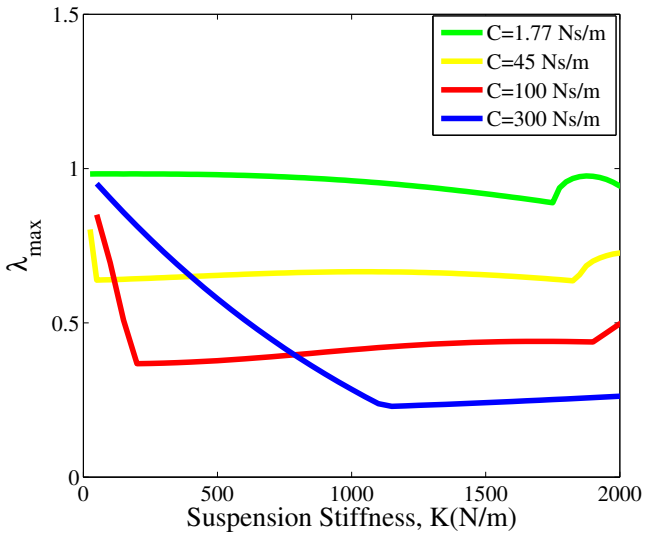

Figure 6.8. Eigenvalues for Low Stiffness Values.

6.3 Discussion

Through this analysis on force dynamics and stability we were able to show the positive aspects of the velocity controlled model over the constant hip torque model.

The marginal variation in the forward speed makes the system more realistic and represents better human locomotion with elastically suspended loads. The stride frequency compares well with the human regime of running with heavy loads as shown by Kram. The main goal of the analysis was to determine which of the two hip actuated models would be a better fit for human locomotion.

The torque profile shows a maximum peak of approximately 440 Nm for all the stiffness values, which can be explained by the fact that this model relies completely on hip actuation with no ankle and knee links. This torque value thus acts as a lumped torque for the model. The RMS value of the torque lies near about 250 Nm, similar to that of the constant torque model.

Hoover et al. showed that, lines of peak forces intersect at a particular stiffness value called the performance stiffness [20]. The velocity controlled model shows a similar trend, however the curves intersect over a region than a point. This result can be attributed to the fact that the stride frequency is constricted within a certain range rather than being constant throughout for all the stiffness values. This can be regarded as an artifact of the velocity controlled Hip actuated SLIP model, as compared to the base excited single mass model used by Hoover et al.

The stability of this system is in close relation to that demonstrated by a hexapod carrying a suspended load [30]. For high damping constants which cause large dissipation of energy, the perturbations decay rapidly, while for low damping the perturbation decay rate is minimized. The eigenvalues tend to lie near the border of the unstable region. A double mass hopper predicted that the stability of legged robots decreases for very low stiffness [30]. We can thus hypothesize that at very low stiffness and low damping the stability is reduced with higher dissipative forces in the system.

7. COMPLIANT POLE DESIGN FOR CARRYING HEAVY LOADS WHILE RUNNING

Elastically suspended loads have been known to reduce shoulder forces during walking and running. Kram et al. showed that carrying 19% of the body weight on bamboo poles while running, reduced peak shoulder forces. The compliance provided by bamboo poles decreases the shoulder forces on the human as compared to a rigid load while running [4]. The loads oscillate about the shoulder due to the excitation provided by human running. Hoover et al. showed that below a certain stiffness the peak shoulder forces are reduced below a certain stiffness. While at resonance theses forces reached their maximum value.

Compliant bamboo poles have been used to carry heavy loads in Asia for generations. Experimental evidence of running with a 15 kg load suspended from a pair of compliant PVC poles shows that such compliant poles act as a vibration-isolating suspension which can reduce the peak forces on the body during locomotion. However, it is not well understood how to choose actual bamboo poles for load carrying to minimize the peak forces on the body. Our objective is to extend the existing experimental evidence using a model of a human running with a load suspended from compliant poles to determine how the effective pole stiffness changes the dynamic forces on the body. Based on stiffness, deflection, and pole mass design constraints, we specify an appropriate range of bamboo dimensions for selecting an appropriate bamboo pole to carry a given load. The simple design methodology presented could simplify the selection of bamboo poles to make it easier to carry heavy loads and reduce the likelihood of musculo skeletal injury.

7.1 Introduction

Carrying loads with compliant load suspensions can significantly reduce the peak forces acting on the body during legged locomotion as compared to a rigidly-attached load [4, 6, 20, 27, 29, 30]. A compliant load suspension essentially acts as a vibration isolator that decouples the motion of the load from that of the body, reducing the peak accelerative forces of the load on the body compared to a rigidly-attached load. In particular, people throughout Asia have been carrying loads during everyday life with very compliant bamboo poles for generations [4]. Such compliant bamboo poles are an ingenious, low-tech solution to help make carrying heavy loads easier over long distances. Kram showed that compliant poles are an effective way to carry heavy loads because they reduce the peak forces on the body and the loading rates while running with a load. Though users are more likely to walk with a load than run with a load, running is a higher-impact activity where compliant bamboo poles are likely to be most beneficial compared to a typical rigid load carrying device, such as a backpack [4]. In Krams experiment, a 15 kg load was carried with two compliant PVC poles that were 3.6 m long with a diameter of 2.54 cm. These poles were oriented symmetrically along the sagittal plane of the body. In practice, pole carriers in Asia are more likely to use various varieties of bamboo, which could have very different geometries and mechanical properties as compared to PVC. Further, instead of using two poles, they may also use one pole oriented on a shoulder in the sagittal plane or along two shoulders in the coronal plane as shown in Figure 7.1.

Our objective in this study is to generalize the excellent results presented by Kram to a more realistic load carrying scenario using compliant bamboo poles and to specify a recommended range of bamboo pole properties for load carrying. Our approach is to use a model of a human running while carrying a load suspended from a compliant bamboo pole using the Hip-Actuated Spring-Loaded-Inverted-Pendulum (SLIP) model to design the properties of bamboo poles such that the peak forces on the body are minimized. We expect that this study can provide simple guidelines

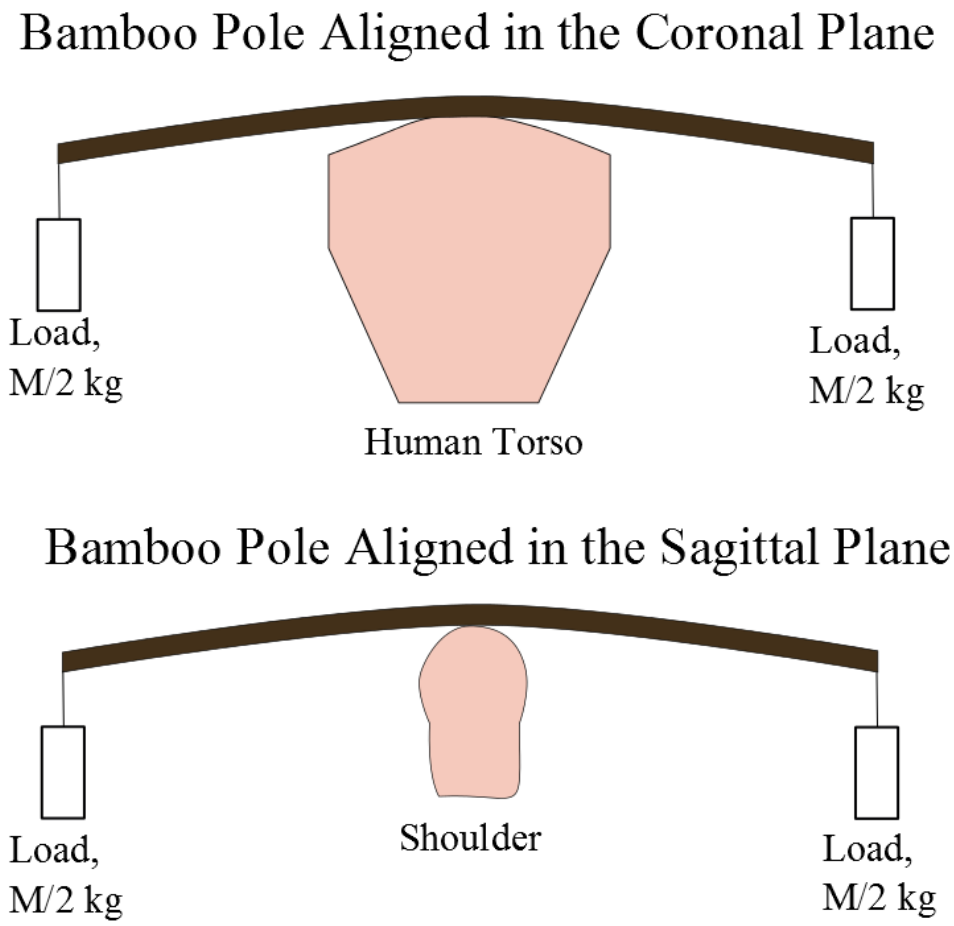

Figure 7.1. Orientation of the Bamboo Pole Along Different Planes.

for the measurement and selection of bamboo poles for carrying heavy loads. If optimal bamboo poles are used for load carriage, the large repetitive forces on the body of carrying heavy loads would be minimized, which would increase comfort and potentially reduce the likelihood of musculo skeletal injury.

7.2 Approach of the Study

7.2.1 General Approach

In order to extend the results by Kram more broadly, we sought to develop and validate a mathematical model that could predict the force results from Kram for human running while carrying a load with compliant bamboo poles. To do so, we chose to use the Hip-Actuated SLIP model with velocity control having a vertical load suspension as it proved to be a highly-stable model and a good approximation of human running. Estimated human parameters based on prior work were used and the natural frequency value specified by Kram was used to calculate the equivalent stiffness of the pole suspension. The peak accelerative shoulder forces of the load on the body were obtained by simulating the model in MATLAB and comparing the model prediction to the experimental results with compliant PVC poles and a rigid backpack [4]. The optimum parameters of a particular bamboo species were evaluated by modeling the bamboo pole as a slender beam and with a symmetric payload attached to either end. To simplify the analysis, we assume that the bamboo pole(s) have negligible mass, though mass is considered later as a design constraint. A recommended region of bamboo pole parameters is determined to minimize the force of the load on the body given realistic design constraints.

7.2.2 Previous Models Used in the Suspended Load study

Various models have been used to study the effects of elastically suspended loads on legged locomotion [6, 24]. Ren et al. developed an advanced model of a human walking with a suspended backpack. A one-degree of freedom vibration model has been shown to predict the forces of load carrying on the human body while walking [20, 29]. The double-mass coupled-oscillator model is capable of similar force predictions as well as energetic predictions of walking with a suspended load [6, 24]. While these models provide an excellent framework from first-principles which can be used to

study locomotion with a suspended load in the vertical direction, more sophisticated models with fore-aft dynamics are required to accurately model human running with a complex coupled interaction between a suspended load and the body for varying suspension parameters. More sophisticated mathematical models of locomotion, such models based on the Inverted Pendulum model of walking and the spring-loaded-inverted-pendulum (SLIP) model of running and walking, have been used in prior work to study human locomotion [7, 18]. Recently, a relatively simple Hip-Actuated SLIP model was developed which is highly-stable and can describe running with realistic human parameters [7, 24]. Unlike the traditional energy-conserving SLIP model, the Hip-Actuated SLIP uses an active torque about the hip to input energy into the system and damping along the leg to release energy in the system [7, 8]. We chose to use this model and modify it with an extra mass atop the actuated mass with a compliant suspension constrained in the vertical direction. A version of this model was originally introduced in a previous conference paper [24].

7.2.3 Speed Controlled Hip Actuated SLIP Model for Running with Compliant Poles

The Hip-Actuated SLIP model [7] is an extension of the classic spring-loaded-inverted-pendulum [8] model with an effective torque about the hip and damping along the leg. Instead of the constant torque model we used a speed controlled model. This model maintains the speed within 2.9 to 3 m/s complying with the speed of human subjects in Kram's paper. A constant torque model is an open loop system which can't maintain a constant speed, thus leading to unrealistic change in speed and stride frequency.

7.3 Significance of the Study

Though bamboo has exceptional mechanical and elastic properties, people were unaware of the optimum parameters required to carry out the activity of load carriage.

For a material used in many structural applications especially it's elastic nature, many parameters are to be considered. The stiffness of a pole is dictated by the length, diameter, thickness and it's modulus of elasticity. Diameter and thickness in bamboo vary based on the type of species [26]. The mechanical properties are influenced by the moisture content in the bamboo [33]. Knowledge about factor of safety against fracture is a must in order to evaluate the design parameters for the bamboo.

Due to lack of options and a low income, this study will provide people in rural areas with necessary information about the measurements of different parameters in bamboo for load carriage. As studies on human subjects have shown that carrying loads decrease the peak shoulder forces on humans. Rigidly attached loads increase the peak shoulder forces to twice the static value. Shoulder forces tend to oscillate about the mean level during walking and running when carrying elastically suspended loads. The design study on bamboo pole modeling will make people aware about the benefits of carrying loads on a compliant pole compared to carrying loads rigidly attached to the body. The comfort of carrying heavier loads with less effect on the human body than usual will prevent occurrence of spinal and vascular injuries among people.

7.4 Selection of Human and Suspension Parameters

7.4.1 Human Parameters

We used approximate human parameters in the model to simulate human running with compliant bamboo poles as shown in Table 7.1. The approximate stiffness of the human leg is dependent on the human stride frequency as showed by Farley et al. [14]. As the stride frequency increases, the leg stiffness increases. Based on this prior work, we selected a suitable value for the effective stiffness of the human leg of 14500 N/m for this particular study. Characteristic behavior of leg damping depends on the viscoelastic properties of the human leg. In prior work, an approximate damping value for the human leg of 950 Ns/m was determined by vertically moving a person

with a harness and fitting the experimental data to a spring-mass-damper model [18]. The human subjects in Kram's experiment weighed approximately 78.8 kg [4], so we used this value to approximate the mass of the human body in the Hip-Actuated SLIP model. A leg landing angle of 65^o was chosen for the model, which is a realistic value for human running [24]. During normal locomotion, humans require a hip torque of around 40-80 Nm, 125-273 Nm at the knee, and 180-240 Nm at the ankle [11]. However, it is not currently known how torque may vary for each leg joints while carrying heavy loads. The torque profile generated due to the speed controlled model lies within the range of human hip torque value. As the model possesses just a single link connecting the mass with the ground, the ankle and knee torques were superimposed onto the hip torque. This helped in better comparison of the superimposed torque with the RMS torque value of the model.

Table 7.1.
Human Parameters Used for the Study.

Parameter	Value
Leg Stiffness, k	14500 N/m
Leg Damping, c	950 Ns/m
Human Mass, m	78.8 kg
Hip Torque, τ	250 Nm
Leg Landing Angle , β	65°.

7.4.2 Suspension Parameters

Approximate parameters were used to model the compliant PVC poles used in the experiments by Kram. These parameters were used to simulate a human running while carrying a 15 kg load suspended from two compliant PVC poles using the Hip-

Actuated SLIP model to compare the experimental and model results. Table 7.2 summarizes these parameters.

Table 7.2.
Evaluated Suspension Parameters.

Parameter	Value
Suspension Stiffness, K	525 N/m
Dashpot Damping, B	1.77 Ns/m
Load Mass, m	15 kg

The compliant poles in Kram's experiment had a natural frequency of $f = 0.94Hz$. Based on this natural frequency we calculated the suspension stiffness using the formula

$$\omega_n = \sqrt{K/M} = 2\pi f. \tag{7.1}$$

Using this formula the stiffness comes out to be $K_{eff} = 525N/m$.

Kram specifies a damping coefficient of 1% or less for the PVC pipes used in the experiment. Hence, the damping ratio of the system is less than 0.01. Damping ration being calculated as

$$\zeta = B/(2\sqrt{KM}). \tag{7.2}$$

This gives us a damping constant of 1.77 Ns/m which decreases the dissipation of energy in the poles. The payload used for the experiment weighs 15 kg equally distributed at each ends. These parameters were used to simulate the motion using the Hip SLIP model and thereby comparing the experimental and modular results.

7.5 Bamboo Pole Design

Bamboo is a natural material with high strength and excellent elastic properties. In sports, bamboo was used for pole vaulting before being replaced by fiber glass.

Many villages across Asia use bamboo as a material for scaffolding due to its high structural rigidity and tolerance. As described previously, people have been known to carry loads suspended from bamboo poles in many parts of Asia. Though bamboo has exceptional mechanical and elastic properties, the optimum parameters required to carry a given load with bamboo poles to minimize the force on the body is not widely known. For a material used in many structural applications particularly for its elastic nature, many parameters are to be considered. The stiffness of a cantilever hollow pole in bending is dictated by its length, diameter, thickness, and modulus of elasticity. The diameter and thickness of bamboo vary based on the type of species [26]. There are over 500 known species of bamboo around the world, so many variations are possible. Further, the mechanical properties of bamboo can be heavily influenced by the moisture content in the bamboo [33], which must be considered. To determine whether a given pole will work without breaking, the factor of safety against fracture should be considered to evaluate the design parameters for the bamboo. In this study, we examine the Kao Zhu and Mao Zhu species of bamboo as they are the most prevalent species found in South East Asia [26]. Their diameters vary from 30-46 mm and 45-86 mm respectively. The thickness is directly proportional to the diameters for Kao Zhu and Mao Zhu and can be expressed as

for Kao Zhu,

$$D_{kz} = 0.31t_{kz} - 6.3, \tag{7.3}$$

for Mao Zhu,

$$D_{mz} = 0.11t_{mz} - 0.6. \tag{7.4}$$

The approximate parameters for both bamboo species are listed in Table 7.3. The parameters may vary for different species of bamboo. It is important to note that the modulus of elasticity for bamboo is approximately 10 times greater than the modulus of elasticity for the PVC pipes, 2.9 GPa, which were used in Krams experiment [4]. Also, since bamboo is naturally available, it will have a fixed diameter range for each species compared to PVC pipes which are manufactured to certain specifications.

Table 7.3.
Approximate Bamboo Parameters. Reproduced from [33].

Parameter	Value
Elastic Modulus , E_{bamboo}	$2.06 * 1^{10} N/m^2$
Ultimate Tensile Strength, σ_{uts}	$193 MPa$
Density, ρ	$0.9 g/cm^3$

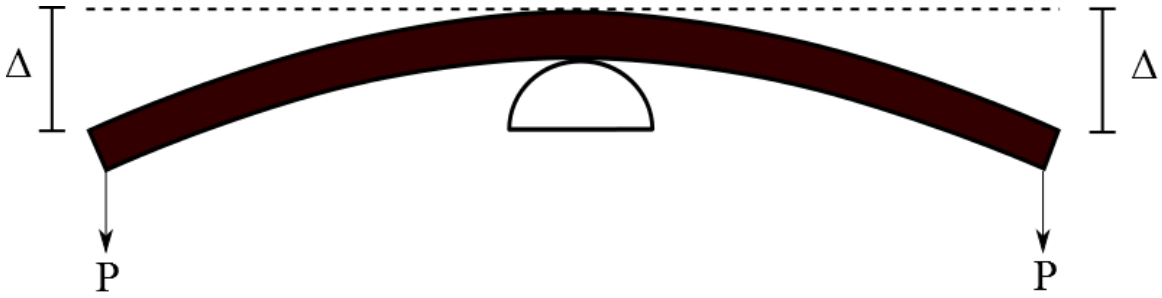

Figure 7.2. Deflection Due to end Loads of the Bamboo Pole.

We considered the bamboo poles to be a hollow cylinder with a constant cross-sectional area. This may not always be a good approximation because some bamboo species can exhibit a considerable taper [26], but here we assume that a bamboo pole with a relatively constant cross section could be obtained. The pole is considered to be a slender beam, which is a good approximation when ten times the pole diameter is much less than the length pole [34]. Hence, the shear modulus G is not considered while calculating the stiffness of the pole.

For symmetric loaded poles, the pole load is given as

$$P = \frac{Mg}{2}. \tag{7.5}$$

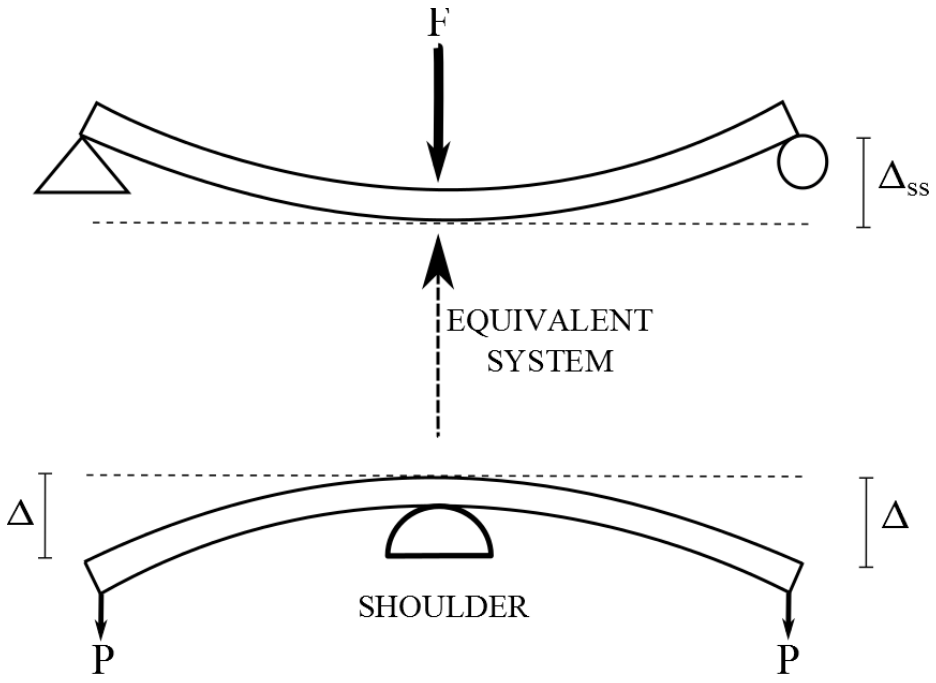

Figure 7.3. Simply Supported Equivalent System for Modeling Bamboo Carried on the Shoulder.

The bamboo pole with support at the midspan is considered to be an equivalent system to a beam simply supported at the end with a point load at the center as shown in the Figure 7.3. The area moment of Inertia of the hollow beam is given by $I = \pi(D^4 - d^4)/64$. Figure 7.4 shows the free body diagram of the bamboo pole in our experiment.

The deflection [35] in a simply supported beam as shown in Figure 7.3 with length L_{ss}, moment of inertia I_{ss} and modulus of elasticity as E_{ss} with a force F at center is given by

$$\Delta_{ss} = \frac{F{L_{ss}}^3}{48E_{ss}I_{ss}}. \tag{7.6}$$

With our bamboo pole the equation upon substituting the given parameters with $L_{ss} = L$, $I_{ss} = I$, $E_{ss} = E$, $F = 2P$ and $\Delta_{ss} = \Delta$.

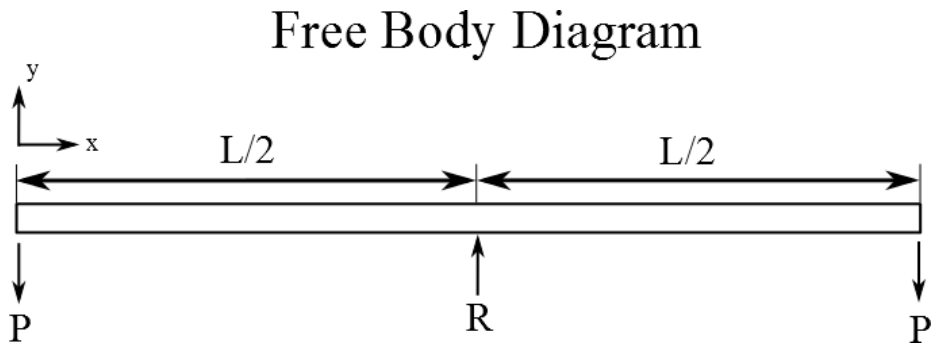

Figure 7.4. Free Body Diagram of the Bamboo Pole.

Upon integration the equation yields $\Delta = 2PL^3/48EI$. Thus, the effective stiffness of the system is given by

$$\frac{2P}{\Delta} = \frac{48EI}{L^3} = K_{eff}, \tag{7.7}$$

where reaction force R due to the shoulder is equal to 2P. The bending moment for

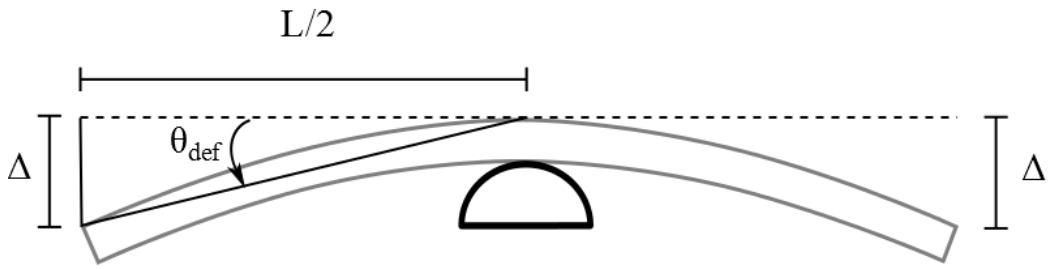

Figure 7.5. Deflection in a Bamboo Pole.

the pole for small deflections is given by

$$\sigma_b = \frac{M_b(\frac{D}{2})}{I}, \tag{7.8}$$

where, $M_b = P(\frac{L}{2})$.

As equation 7.8 relies only on small deflections in beam, this equation was also considered as an approximation for deflections occurring in the bamboo pole in order

to avoid complexity of elliptical integrals. As the beam bends more it becomes more non linear which makes the beam stiffer. The deflection in bamboo is shown in Figure 7.5. The angular deflection θ_{def} is calculated as

$$\theta_{def} = \tan^{-1}(\frac{\Delta}{L/2}). \tag{7.9}$$

To ensure that the recommended range of bamboo pole parameters would work in practice without snapping, the factor of safety against fracture of the pole due to excessive bending stress was calculated. As the bending moment is directly proportional to the pole length, the critical constraint to be assessed is due to the maximum deflection of the pole:

$$n_{fracture} = \frac{\sigma_{uts}}{\sigma_b} \tag{7.10}$$

was used to evaluate the safety factor for bamboo poles.

7.6 Results

7.6.1 Model Validation

The Hip-Actuated variable torque SLIP model has velocity control and the velocity varies marginally as the stiffness is varied from 25 N/m to 1775 N/m. The velocity fluctuates from 2.9 m/s to 3 m/s while the stiffness is varied. The model trajectories of a human running with a load suspended from compliant poles is very similar to the actual experimental results reported by Kram. Figure 7.6 shows the closeness of the results obtained using the velocity controlled model and Kram's result. The slight variation in the body trajectory w.r.t. time is due to slight error in velocity value.

Further, the models peak force predictions for a human running while carrying a load with compliant poles and a rigid backpack are very similar to the actual experimental results reported by Kram as shown in Figure 7.7. The rigid backpack puts approximately twice as much peak force on the shoulders compared to the compliant poles. With compliant poles, the forces of the load on the body oscillate between

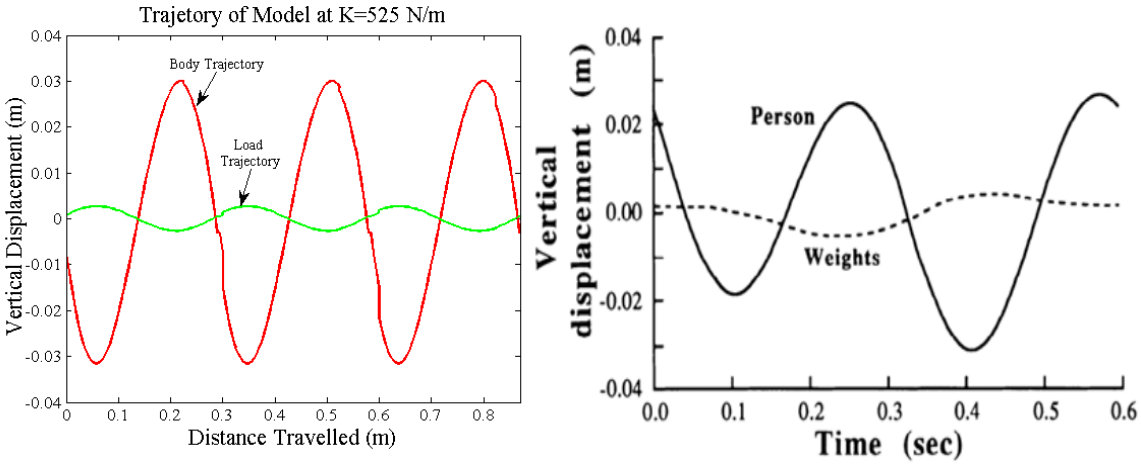

Figure 7.6. (Left) Model Trajectory at K=525 N/m. (Right)Trajectory of Body Center Obtained by Kram, reproduced from [4].

120-180 N in the experiment by Kram and between 130-170 N in the Hip-Actuated SLIP model prediction.

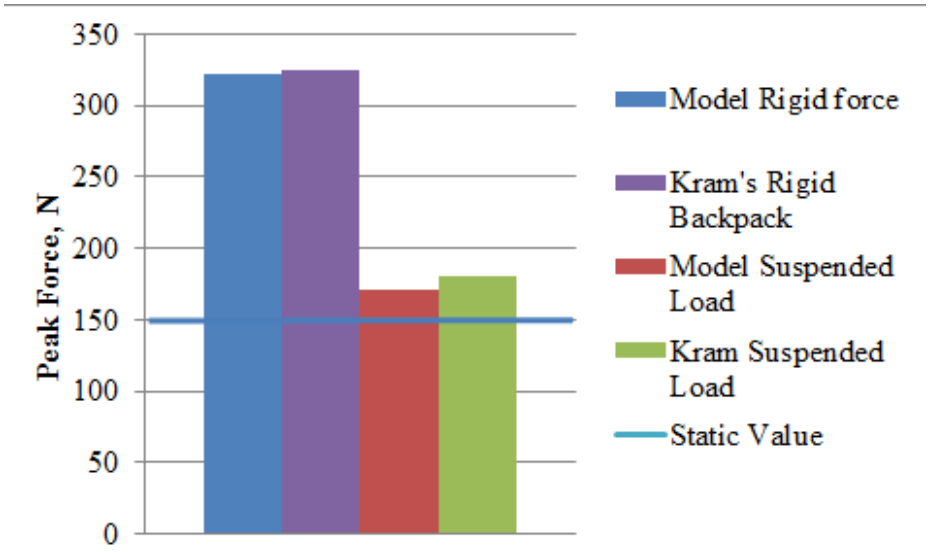

Figure 7.7. Comparison Between Model and Experimental Results for Rigid and Suspended Load.

7.6.2 Bamboo Pole Design and Optimization

In order to optimize the bamboo pole design, we added a few constraints to the pole parameters. This optimization helps bound the stiffness range of the bamboo pole and establish a recommended range of pole parameters such that the force of the load on the body from carrying a load would be substantially reduced. The maximum stiffness value K_{max} was determined by capping the peak shoulder force at 150% of the static load force value (i.e. 1.5(150 N) = 225 N). This maximum stiffness value was estimated to be 1775 N/m by the Hip-Actuated SLIP model. The minimum stiffness K_{min} value was calculated by restricting the maximum deflection of the bamboo pole to half the average height of the carrier i.e. approximately 0.8 m [36]. This constraint would ensure a reasonable ground clearance for a load to be carried without hitting the ground. From Equation 7.7, for a 15 kg load this minimum value of K_{min} is 150/0.8=183.75 N/m. The third constraint is based on the mass of the pole. We assume that the pole mass of less than 2 kg, or approximately 13% of a 15 kg payload, can be considered to be negligible. If the added pole mass is higher than 2 kg, the added bamboo pole mass starts to become considerable. Further, we assume that the bamboo pole behaves as a massless slender beam to simplify the analysis. Distributed mass systems have multiple modes of vibration and considering the effect of the added pole mass could make the analysis and recommendations more complicated than necessary. Based on the chosen K_{min} and K_{max} values, the minimum and maximum pole length limits were evaluated using Equations 7.11 and 7.12 respectively. The K_{eff} values were halved when using this equation to account for the pole being supported on the shoulders at the midspan. Hence, the length of the pole for the given range of Kao Zhu diameters (30-46 mm) and Mao Zhu diameters (45-86 mm) can be determined using

$$L_{min} = \sqrt[3]{\frac{48EI}{K_{max}}}, \tag{7.11}$$

$$L_{max} = \sqrt[3]{\frac{48EI}{K_{min}}}. \tag{7.12}$$

Based on the above constraint calculation we plot the recommended region for the species Kao Zhu. A fairly big set of length and diameter values can be utilized to obtain a suitable bamboo pole required to carry a load of 15 kg as seen in Figure 7.8

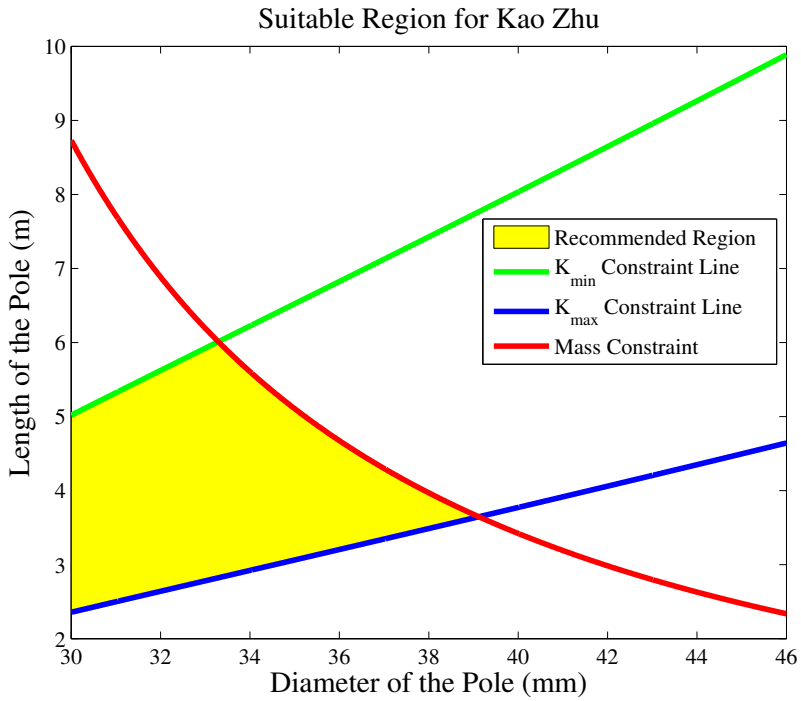

Figure 7.8. The Yellow region is the identified Suitable Region for which the Shoulder Peak Forces will Lie within the Constraints for Kao Zhu.

Similarly for the Mao Zhu species the region shrinks to a very small area as seen in Figure 7.9. This arises due to the fact that the diameter range of Mao Zhu is almost twice as large as that of Kao Zhu. This causes increase in length of the beam as lengths are proportional to $I^{(1/3)}$ or $D^{(4/3)}$ as seen in Equation 7.11 and 7.12.

In order to gain a fair idea of the narrow region of the Mao Zhu species we zoom in to observe the optimized parameter values. Figure 7.10 shows the narrow region.

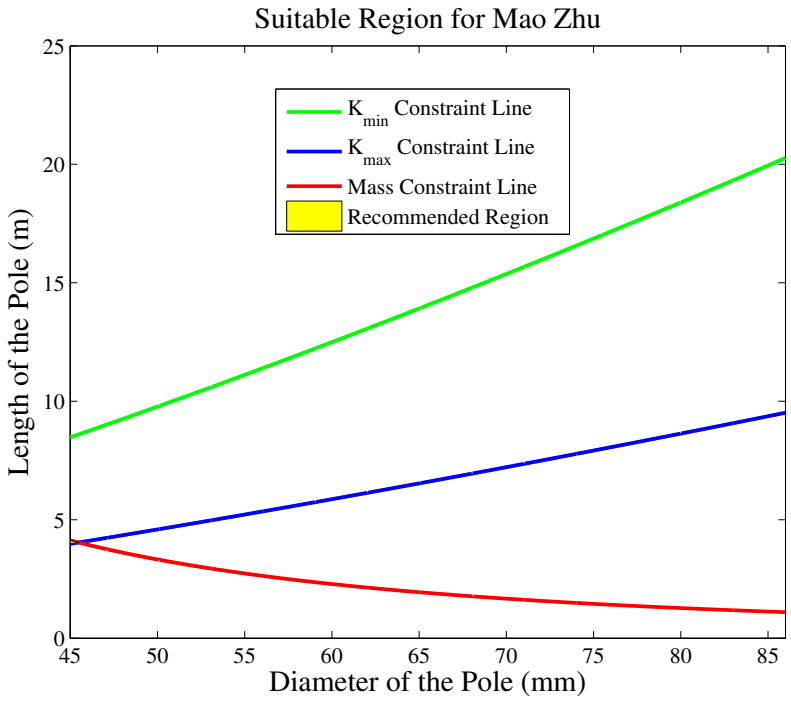

Figure 7.9. The Yellow region is the identified Suitable Region for which the Shoulder Peak Forces will Lie within the Constraints for Mao Zhu. As we see due to the Increase in Diameter of the Bamboo there is a Significant Shrinking of the Recommended Region.

7.6.3 Bamboo Deflection and Factor of Safety

As the bending stress value is suitable for small angular deflection of the beam, we evaluated the angular deflection that the beam undergoes for both Kao Zhu and Mao Zhu. Due to the increase in length observed in Mao Zhu the angular deflection decreases as compared to Kao Zhu. The maximum deflection undergone by Kao Zhu is around 18^o which can be considered as a approximately small deflection. Hence, from Figure 7.8 it would be preferable to use larger length values within the recommended region as it would provide a better estimate of stress in the beam. This would in turn provide a more accurate factor of safety value as safety factor values too depend on the bending stress values. To ensure safety against fracture the the pole lengths

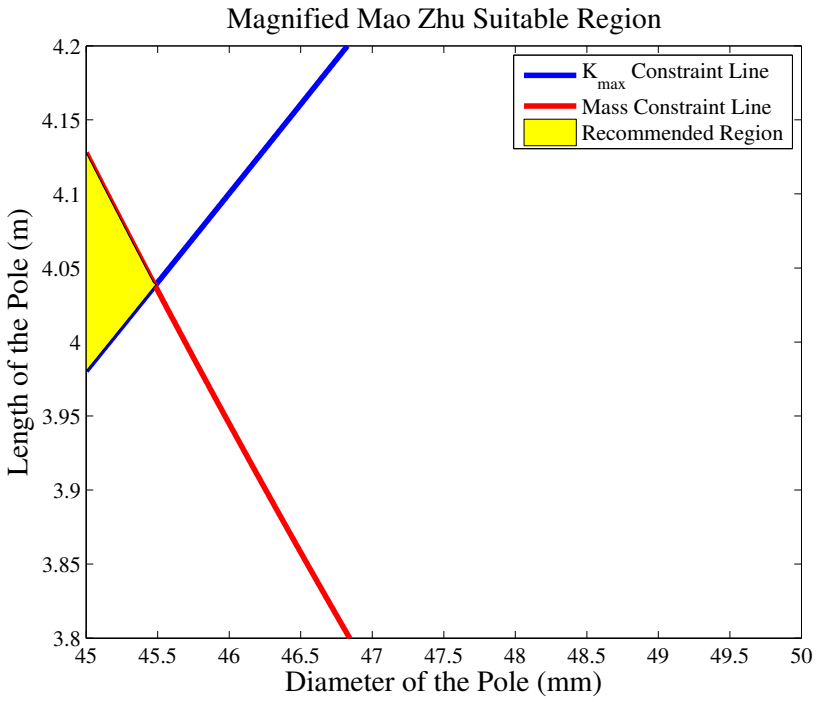

Figure 7.10. Figure 7.9 Magnified to Observe the Suitable Region for Mao Zhu.

were tested for their structural rigidity against snapping. Mao Zhu having a lower bending stress due to larger diameter range as compared to Kao Zhu showed better resistance against fracture for increasing length of the pole. A factor of safety of 2 is considered safe for beam and shaft design [35]. Thus, the Kao Zhu lengths were considered within safe range as seen in Figure 7.13

For Mao Zhu the least factor of safety was equal to 5. This was higher as compared to Kao Zhu minimum value. Figure 7.14 show the trend of factor of safety for the species Mao Zhu.

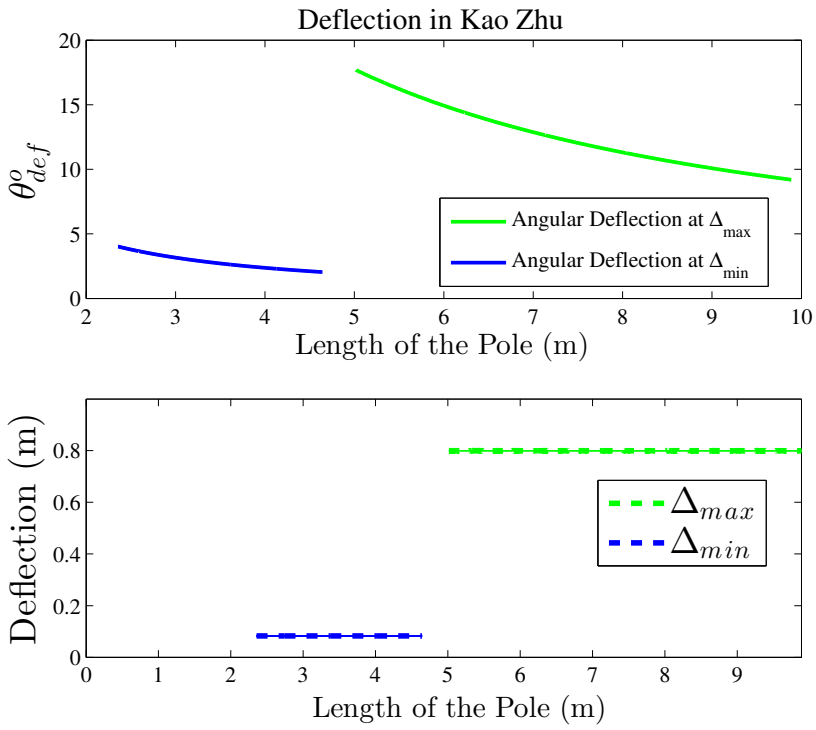

Figure 7.11. Plot Showing the Angular Deflection Underwent by Kao Zhu as the Pole Length is Increased. The Plot Subplot shows the Constant Deflection as would be the Case for a Constant Stiffness Value.

7.6.4 Shoulder Force Trend for Varying Pole Stiffness

Upon fixing the upper and lower limit of the K_{eff} values, a trend line showing the peak forces of the load acting on the body for different suspension stiffness values was generated using the Hip-Actuated SLIP model. This trend in the peak forces was then compared to the experimental value showed by Kram along with the rigid backpack force value and static load value Figure 7.15. It is evident that as the stiffness of the pole suspension is minimized, the peak shoulder force approaches the static load value. At K = 525 N/m, the model is able to predict the experimental result from Kram with a difference in peak force value of 10 N.

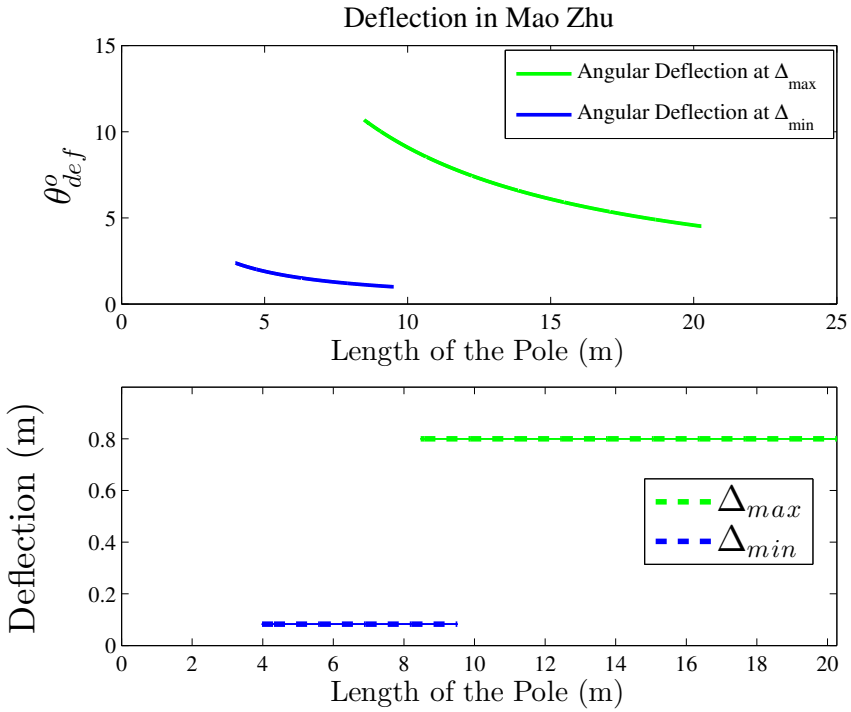

Figure 7.12. Plot Showing the Angular Deflection Underwent by Mao Zhu as the Pole Length is Increased. The Plot Subplot shows the Constant Deflection as would be the Case for a Constant Stiffness Value.

7.7 Discussion

7.7.1 Overall approach

In the paper, we have validated a realistic model of human running while carrying a load with compliant poles using existing experimental evidence. We then extended this model to show how different effective bamboo pole stiffness values could minimize the peak forces acting on the body while carrying a 15 kg load. To design bamboo poles with these desired effective pole stiffness values, we provided a recommended region of pole lengths and diameters for the Kao Zhu bamboo species.

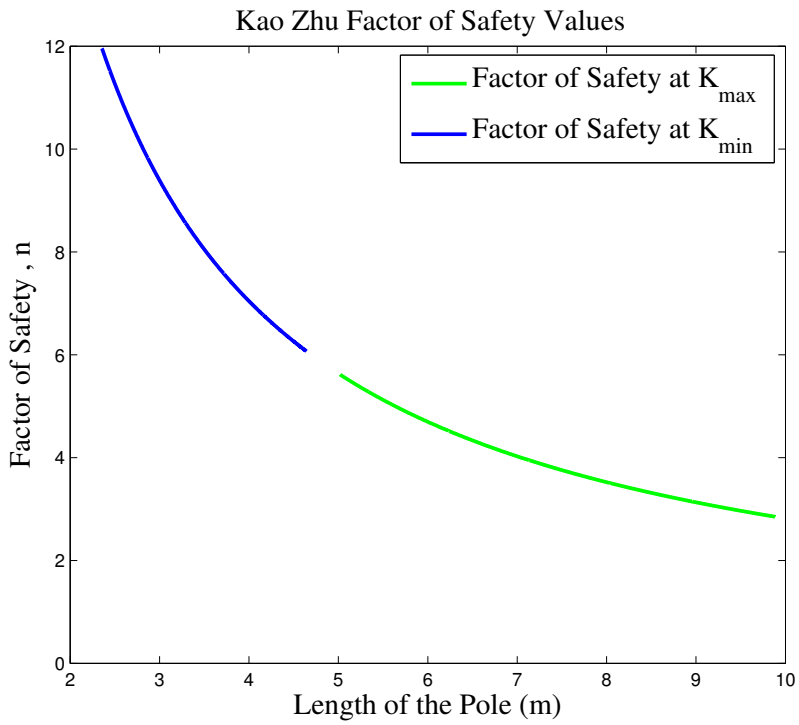

Figure 7.13. Plot Showing Factor of Safety Trend for Kao Zhu with the Largest Pole Length having the Least Factor of Safety.

7.7.2 Walking versus Running

In the present study, we considered running while carrying a load with compliant bamboo poles. This represents a worst-case scenario because running provides greater vertical displacements and higher peak forces than walking [4]. If one is walking while carrying a load with compliant bamboo poles instead of running, then the acceptable maximum pole stiffness value K_{max} would be reduced because the stride frequency of walking is lower than that of running. Thus, it would be even more important to select a compliant bamboo pole close to the minimum pole stiffness value K_{min} that was specified to isolate the motion of the load from the body and to minimize the peak forces acting on the body.

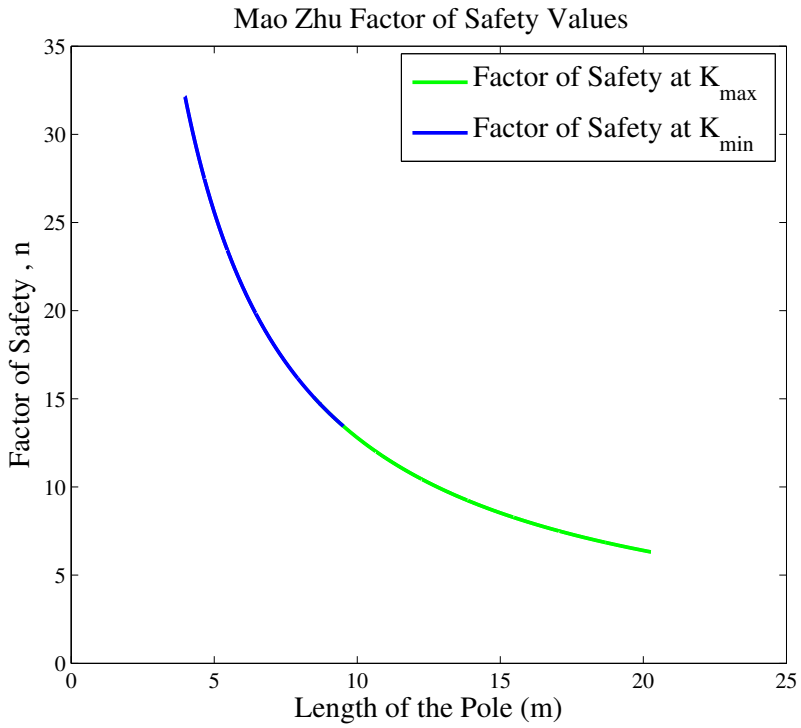

Figure 7.14. Plot Showing Factor of Safety Trend for Mao Zhu with the Largest Pole Length having the Least Factor of Safety.

7.7.3 A Simple Bamboo Pole Tuning Strategy

It is clear from the model results that minimizing the effective bamboo pole stiffness is desirable to minimize the peak forces acting on the body. Therefore, a simple way to pick an appropriate bamboo pole to carry a given load would be to start with a very long bamboo pole (3-4 m long) and tie the desired load to be carried symmetrically on each end and to observe the deflection when carried. One can then move the loads on each end closer until a reasonable ground clearance is obtained and the poles statically deflect to about half of the individuals height. Any excess pole length left over can be cut off and the poles will be appropriately tuned to minimize the peak forces acting on the body.

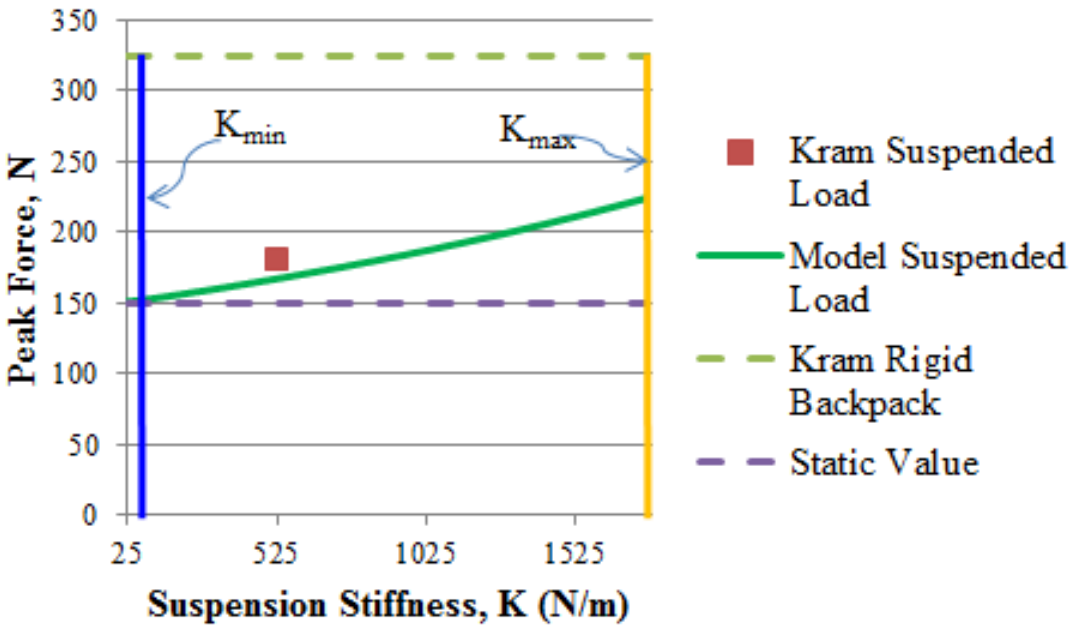

Figure 7.15. Model Predictions of the Peak Shoulder Forces Over a Range of Effective Pole Stiffness Values.

7.7.4 Changing Load Mass

If the load masses to be carried by bamboo poles are likely to change substantially, then bamboo poles with different properties may have to be used. In the present paper, we considered a 15 kg load, which at the minimum stiffness K_{min} would cause the poles to deflect by approximately half of the body height. If a 30 kg load is to be carried with the same bamboo poles optimized for carrying 15 kg, the pole will likely be too compliant and deflect too much to effectively carry the 30 kg load. A simple solution in this case would be to double the effective pole stiffness by using two of the same bamboo poles that were used to carry 15 kg. If the use of one pole is desired, then a stiffer bamboo pole with a shorter length and/or larger diameter would have to be used. If a 7.5 kg load is to be carried the same bamboo poles, then the poles optimized for carrying a 15 kg load may be too stiff. It may be desirable to use a

longer pole with a smaller diameter to carry the 7.5 kg load. Another possible solution to the problem of changing load mass is to attach or tie the loads at varying points along the bamboo pole. That way, the effective stiffness of the pole can be varied for different load mass values. The effective stiffness can be increased by attaching the load further from each end of the pole and the effective stiffness can be decreased by attaching the load closer to each end the pole.

7.7.5 Shoulder Harnessing Technique

In this study, we assumed that a single bamboo pole is to be carried on the shoulders in the sagittal plane. If the pole and load are carried along one shoulder in the sagittal plane, asymmetric dynamic loading on the body may result [4]. This potential effect is neglected in our model, but would likely affect the dynamics of carrying loads with compliant poles. As in Krams experiment, two poles could be carried on the shoulders along the sagittal plane with one on each shoulder. Two identical poles in parallel would double the effective stiffness of the compliant poles, so longer poles would be required to achieve the same K_{min} value as that of a single pole. The double pole configuration may be particularly helpful for carrying even larger load masses. A single bamboo pole can also be carried on the shoulders along the medial plane. This would result in a longer distributed support over the shoulders behind the head and would likely be more comfortable than a single pole on one shoulder. The analysis in this paper would also apply to this carrying configuration, but the pole may need to be slightly longer to account for the larger pole shoulder support. Knapik et al. mentions that a wider shoulder strap of a backpack better the load distribution and less pressure on the skin [5]. Hence, a pole with larger diameter will help distribute the pole load on a larger contact area of the pole. Further, a pole carried along the shoulder oriented in the medial direction will likely result in better load distribution. Knapik et al. also mentions that a front and back backpack will help in equally distributing load which will lead in more effective load carriage and

prevent leaning [5]. This also puts less pressure on the back muscles as compared to backpacks.

7.7.6 Limitations of Compliant Pole Analysis

A relatively simple analysis approach was used to determine a range of parameters to design a bamboo pole for load carrying. However, it is important to note some of the potential limitations of the simplified analysis methodology presented. In the derivation of the beam deflection, effective stiffness, and stress, we assumed that the compliant bamboo pole experiences pure bending. This is an appropriate assumption when the poles are very long because they would experience a relatively low angular displacement even with a deflection as large as half of the body height. For the shorter poles closer to 1 m, the angular deflection may be too large to use a linear approximation for a slender beam in pure bending. The analysis of large-deflection beams requires a more complex approach, but we did not explore the characteristics of relatively short bamboo poles with large-deflections because longer, more compliant poles that are closer to the linear bending approximation are more desirable for load carrying. The minimum stiffness value K_{min} was determined from an assumed minimum deflection of half of the body height primarily to ensure the load could be carried with an appropriate ground clearance. It is possible that larger deflections could be achieved and which would provide even more compliant suspensions that transfer less force to the body, but there are diminishing returns. Therefore, we chose to constrain the maximum deflection to an easily measurable deflection by referencing ones own body height (which would vary slightly with differences body heights). The compliant bamboo poles were assumed to be slender, massless beams. In reality, the compliant poles do act as a beam with a distributed mass which would require our analysis to be modified. Since we constrained the mass of the beams to 2 kg or less, which is only 13.3 % of the 15 kg load, the massless assumption will give a good

approximation. For heavier poles, the effect of a distributed pole mass may need to be considered.

The variable torque model uses a torque profile in order to keep the velocity near the target range. In this case the target horizontal speed being 3 m/s. It ensures that the velocity does not waver off too much from the desired value. There is an offset of at most 0.1 m/s. Compared to the constant torque model, variable torque provides more stable and accurate results.

8. CONCLUSION

A double mass hip actuated SLIP with constant torque is able to predict certain characteristics of the body and load dynamics of locomotion with suspended load. However, the increase of speed upon increment in suspension stiffness is an anomaly showed by this model. It is capable of showing reduction in peak forces due to a suspended load but not reduction in power.

A velocity controller added to this constant torque model provides the necessary feedback control required to run at a constant speed unlike the previous model with no regulation. There still lies marginal error in the forward speed of the human which may arise from the fact that a human also changes his or her leg angle while trying to run at constant speed as the stiffness is varied.

Both the constant torque and velocity control model show that for low suspension stiffness the system becomes less stable as the eigenvalues lie along the border separating stable and unstable region. A variable damping for the suspension can provide necessary dissipation of energy of perturbations. Tuning for resonance is required so as to decrease the transmissibility and magnification of load amplitude as seen in the velocity control model. To address both these stability issues a semi active suspension incorporating a linear elastic actuator could prove to be beneficial in decoupling the load and the body mass. This could help in providing necessary stability for the low stiffness and the resonance region.

A compliant bamboo pole is an inexpensive method for carrying heavy loads elastically. Optimizing design parameters of the bamboo provides knowledge of the requisite parameters to make a bamboo pole comply to the performance limits of load suspensions. There are around 500 bamboo species found in nature and not all of them are capable of meeting needs of both flexibility and structural rigidity. This

study can help analyze every such species in detail and optimize their parameters to fit the needs of carrying heavy loads.

Suspended elastic loads in place of rigidly attached loads have advantages as seen in this study. They not only increase the comfort on the person carrying it but also provide prevention from musculo skeletal injuries.

LIST OF REFERENCES

LIST OF REFERENCES

[1] Renee L Attwells, Stewart A Birrell, Robin H Hooper, and Neil J Mansfield. Influence of carrying heavy loads on soldiers' posture, movements and gait. *Ergonomics*, 49(14):1527–1537, 2006.

[2] R McNeill Alexander. *Elastic mechanisms in animal movement*. Cambridge: Cambridge University Press, 1988.

[3] Y Epstein, LA Stroschein, and KB Pandolf. Predicting metabolic cost of running with and without backpack loads. *European journal of applied physiology and occupational physiology*, 56(5):495–500, 1987.

[4] R. Kram. Carrying loads with springy poles. *Journal of Applied Physiology*, 71(3):1119–1122, 1991.

[5] Joseph Knapik, Everett Harman, and Katy Reynolds. Load carriage using packs: A review of physiological, biomechanical and medical aspects. *Applied ergonomics*, 27(3):207–216, 1996.

[6] Jeffrey Ackerman and Justin Seipel. Energetics of bio-inspired legged robot locomotion with elastically-suspended loads. In *Intelligent Robots and Systems (IROS), 2011 IEEE/RSJ International Conference on*, pages 203–208. IEEE, 2011.

[7] ZH Shen and JE Seipel. A fundamental mechanism of legged locomotion with hip torque and leg damping. *Bioinspiration & Biomimetics*, 7(4):046010, 2012.

[8] Justin E Seipel and Philip Holmes. Running in three dimensions: Analysis of a point-mass sprung-leg model. *The International Journal of Robotics Research*, 24(8):657–674, 2005.

[9] *Human Body Planes*. 2013 (accessed November 23, 2013).

[10] Jerry Krause. Biomechanics: A qualitative approach for studying human movement. *Quest*, 38(1):80–81, 1986.

[11] Harrison P Crowell III, Angela C Boynton, and Michael Mungiole. Exoskeleton power and torque requirements based on human biomechanics. Technical report, DTIC Document, 2002.

[12] Richard E Seroussi, Andrew Gitter, Joseph M Czerniecki, and Kelly Weaver. Mechanical work adaptations of above-knee amputee ambulation. *Archives of physical medicine and rehabilitation*, 77(11):1209–1214, 1996.

[13] *Muscle Network in the Leg*, 2013 (accessed November 23, 2013). `http://25.media.tumblr.com/tumblr_mdrqjsihxa1rlyzj6o1_r1_500.jpg`.

[14] Claire T Farley and Octavio Gonzalez. Leg stiffness and stride frequency in human running. *Journal of biomechanics*, 29(2):181–186, 1996.

[15] Adamantios Arampatzis, Gert-Peter Brüggemann, and Verena Metzler. The effect of speed on leg stiffness and joint kinetics in human running. *Journal of biomechanics*, 32(12):1349–1353, 1999.

[16] Svetlana Rapoport, Joseph Mizrahi, Eitan Kimmel, Oleg Verbitsky, and Eli Isakov. Constant and variable stiffness and damping of the leg joints in human hopping. *Journal of biomechanical engineering*, 125(4):507–514, 2003.

[17] Daniel P Ferris, Micky Louie, and Claire T Farley. Running in the real world: adjusting leg stiffness for different surfaces. *Proceedings of the Royal Society of London. Series B: Biological Sciences*, 265(1400):989–994, 1998.

[18] L Zhang, Dali Xu, Mohsen Makhsous, and Fang Lin. Stiffness and viscous damping of the human leg. In *Proceedings of the 24th Annual Meeting of the American Society of Biomechanics*, 2000.

[19] Riddle S. *Modeling Tools for Conformal Orthotic Devices*. Master's thesis, Purdue University.

[20] J Hoover and SA Meguid. Performance assessment of the suspended-load backpack. *International Journal of Mechanics and Materials in Design*, 7(2):111–121, 2011.

[21] Sharifah Alwiah Abdul Rahman, Azmin Sham Rambely, and Rokiah Rozita Ahmad. Effect of load carriage on the backpack vibration system. *Applied Mechanics and Materials*, 165:295–299, 2012.

[22] Justin Seipel and Philip Holmes. Three-dimensional translational dynamics and stability of multi-legged runners. *The International Journal of Robotics Research*, 25(9):889–902, 2006.

[23] Justin E Seipel and Philip J Holmes. Three-dimensional running is unstable but easily stabilized. In *Climbing and Walking Robots*, pages 585–592. Springer, 2005.

[24] Ackerman Jeffrey Potwar, Karna and Justin Seipel. Actuated model of human running with an elastically suspended load. In *Proceedings of the ASME 2013 International Design Engineering Technical Conferences Computers and Information in Engineering Conference*. ASME, 2013.

[25] Marilee J Stephens and Jaynie F Yang. Loading during the stance phase of walking in humans increases the extensor emg amplitude but does not change the duration of the step cycle. *Experimental Brain Research*, 124(3):363–370, 1999.

[26] Tommy Y Lo, HZ Cui, and HC Leung. The effect of fiber density on strength capacity of bamboo. *Materials Letters*, 58(21):2595–2598, 2004.

[27] Lawrence C Rome, Louis Flynn, and Taeseung D Yoo. Biomechanics: Rubber bands reduce the cost of carrying loads. *Nature*, 444(7122):1023–1024, 2006.

[28] Xu Xu, Simon M Hsiang, and Gary A Mirka. The effects of a suspended-load backpack on gait. *Gait & Posture*, 29(1):151–153, 2009.

[29] Matthieu Foissac, Guillaume Y Millet, André Geyssant, Philippe Freychat, and Alain Belli. Characterization of the mechanical properties of backpacks and their influence on the energetics of walking. *Journal of biomechanics*, 42(2):125–130, 2009.

[30] Jeffrey Ackerman and Justin Seipel. Coupled-oscillator model of locomotion stability with elastically-suspended loads. ASME, 2011.

[31] Yuri P Ivanenko, Francesca Sylos Labini, Germana Cappellini, Velio Macellari, Joseph McIntyre, and Francesco Lacquaniti. Gait transitions in simulated reduced gravity. *Journal of Applied Physiology*, 110(3):781–788, 2011.

[32] Steven H. Strogatz. *Non Linear Dynamics and Chaos*. 1994.

[33] SC Lakkad and JM Patel. Mechanical properties of bamboo, a natural composite. *Fibre Science and Technology*, 14(4):319–322, 1981.

[34] Ansel C Ugural and Saul K Fenster. *Advanced strength and applied elasticity*. Pearson Education, 2003.

[35] Richard Gordon Budynas and J Keith Nisbett. *Shigley's mechanical engineering design*. McGraw-Hill New York, 2008.

[36] Angus Deaton. Height, health, and development. *Proceedings of the National Academy of Sciences*, 104(33):13232–13237, 2007.